Structural Durability & Health Monitoring

Tech Science Press

Doi:10.32604/sdhm.2025.075535

ARTICLE

Low Cost Friction Damper Solutions for Seismic Performance Enhancement of Structures

Radha Krishna Mallik[1], **Gokarna Bahadur Motra**[1] **and Krishna Shrestha**[2,3,*]

[1]Department of Civil Engineering, Institute of Engineering Pulchowk Campus, Tribhuvan University, Lalitpur, 44700, Nepal
[2]Centre for Infrastructure Engineering, Western Sydney University, Penrith, NSW 2751, Australia
[3]Fujian University of Technology, Fuzhou, 350000, China

*Corresponding Author: Krishna Shrestha. Email: k.shrestha@westernsydney.edu.au

Received: 03 November 2025; Accepted: 19 December 2025; Published: 18 May 2026

ABSTRACT: The study proposes a low-cost friction damper designed to enhance the seismic performance of buildings, particularly in regions where existing structures lack adequate seismic resistance and conventional friction dampers are cost-prohibitive or require specialized fabrication. Friction dampers are displacement-controlled devices that dissipate energy through constant slip-force action and relative displacement between attachment points, typically ensuring elastic structural behavior under Design Basis Earthquake (DBE) demands and controlled yielding under Maximum Considered Earthquake (MCE) conditions. To address limitations in current practice, the proposed device integrates the damping mechanism of vehicle leaf-spring suspension systems with rotational plate friction interfaces activated through bolt pretension, enabling fabrication from commonly available structural components. The device's energy dissipation arises from friction between leaf-spring plates, friction across rotational plates, and deformation of the leaf springs, each of which is examined to characterize overall behavior. Numerical modeling incorporating contact non-linearity verifies the force–deformation response, and the equivalent viscous damping ratio is estimated to evaluate performance. Results demonstrate that the proposed Leaf Spring–Rotational Plate (LSRP) friction damper provides substantial energy dissipation capacity, offering a practical and affordable seismic retrofit solution for buildings not originally designed for lateral loads. Comparison between theoretical predictions and numerical simulations confirms the accuracy of the proposed formulation in capturing the damper's hysteretic behavior, establishing a foundation for future investigation of its performance across structures with varying dynamic characteristics.

KEYWORDS: Friction damper; strengthening; energy dissipation by friction; external leaf spring; rotational sliding plates; contact non-linearity numerical model; equivalent viscous damping ratio

1 Introduction

Many existing building structures were not originally designed to resist lateral loads induced by ground motion. Even among those that were designed for lateral loads, a significant number no longer satisfy current code-specified performance requirements, making performance enhancement necessary for design-level earthquakes. Traditional seismic retrofitting methods typically involve major structural interventions, which may require the building to be taken out of service during construction.

An alternative approach is to reduce the seismic demand on the structure rather than increasing the capacity of its lateral load-resisting elements through larger member sizes or additional reinforcement. This can be achieved by incorporating energy-dissipating systems into the structure. Such systems, commonly

known as dampers, help dissipate input seismic energy and thereby reduce the lateral force demand on the primary structural components.

Seismic effects induce lateral inertial forces proportional to tributary mass and the induced acceleration at the level of mass. The amplitude of the lateral acceleration and displacement induced by an earthquake is proportional to the input energy from ground shaking. In the absence of the seismic energy dissipating devices, this input energy is dissipated through inelastic deformation of the structural elements [1].

According to Pall and Marsh [2], this criterion of energy dissipation by structural elements undergoing inelastic deformation attracts significant damage and the cost of repairing such damage may be up to the cost of replacing collapsed structures.

To reduce inelastic deformation in structures, it is necessary to attach an additional energy dissipation system outside the structure. Thus, every year, new types of energy dissipating systems emerge as research outputs.

Fig. 1 shows the broad classification of energy-dissipating systems: active, semi-active, and passive systems used for energy dissipation in structures. The characteristic feature of passive energy-dissipating systems is energy dissipation through the hysteretic behavior of the cyclic force–displacement response, where the area enclosed by the hysteresis loop represents the energy dissipated per cycle [2–6].

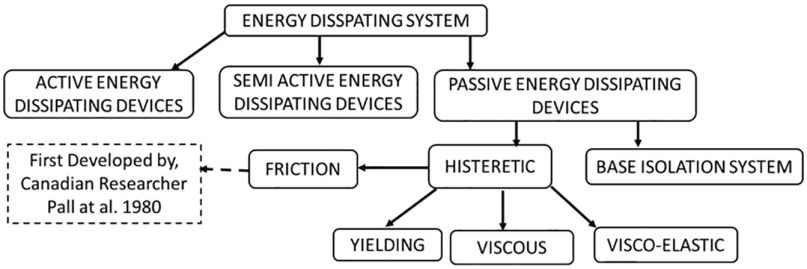

Figure 1: Broad classification of energy dissipation systems used in structures. Among the various categories of hysteretic dampers, friction dampers are displacement-sensitive devices that operate at a constant slip force. Friction dampers are passive energy-dissipating devices with energy dissipation through hysteretic force-deformation response

According to Constantinou and Symans [7], there has been a rapid implementation of passive energy-dissipation systems for seismic applications since the mid-1990s. The main aim of the passive energy-dissipation system is to reduce the inelastic deformation of the structural elements of the structure.

Yield, viscous, and friction dampers are the most frequently used dampers. Yield dampers used as bracing elements have localized yielding zones with significant energy dissipation capacity [8–10].

Yielding viscous dampers used as bracing elements can undergo strain hardening, which necessitates designing for higher force demands without applying overstrength reduction factors to non-dissipative structural components. Additionally, concerns have been raised regarding the potential for residual deformations and the development of soft-story mechanisms following seismic events [11,12].

Viscous dampers are velocity-sensitive devices, and their properties change with the change in temperature due to the temperature sensitivity of the viscous material used in the damper [13,14]

Pall [15] stated that friction dampers are displacement-sensitive devices, and numerous configurations have been developed to enhance the seismic performance of structures. Pall introduced limited-slip bolted joints, in which pretensioned bolts generate frictional resistance between sliding plates. The energy is dissipated through the frictional forces that act as the plates undergo relative displacement at the damper location.

Filiatrault et al. [16] developed friction-spring dampers that utilize ring springs as the primary components for dissipating seismic energy. The resulting force–displacement hysteresis loops were self-centering, repeatable, and stable, with identical behavior in tension and compression and minimal variation across the frequencies considered. The damper was also found to be effective in reducing acceleration demands during earthquake intensities that would otherwise cause slight yielding in an undamped structure.

Filiatrault and Cherry [17] also proposed friction-damped braced frame (FDBF) systems, in which the braces are connected through slip-critical joints. In this configuration, the bracing members are activated under both tensile and compressive diagonal forces, allowing the system to dissipate energy effectively during seismic loading.

Aiken et al. [18] tested a 9-story, quarter-scale friction damped braced Frame (FDBF) structure under various ground-motion records and reported a substantial improvement in seismic performance due to the inclusion of friction damping devices. The devices significantly increased the effective damping of the structure, resulting in improved overall response. The friction mechanisms demonstrated reliable energy-dissipation characteristics and were not damaged even under large load demands. Moreover, the devices became increasingly effective as the intensity of the seismic forces increased. By concentrating energy dissipation within these purpose-designed friction devices—capable of sustaining extreme loading without damage—the primary structural elements were able to remain essentially elastic [19].

From an analytical perspective, passive energy dissipators can be broadly classified into two major categories: viscous dampers and friction-type dampers. Material-yielding devices exhibit hysteretic behavior similar to that of frictional systems. In contrast, tuned mass dampers are not true energy dissipators, as they merely store kinetic energy without dissipating it.

Viscous dampers offer analytical advantages due to their linear, velocity-proportional behavior; however, they are unable to resist static or slowly applied loads, including gravity loads. Friction-type dampers, although nonlinear in behavior, being dependent on both displacement and slip force, are capable of resisting both static and dynamic loading.

One notable friction-based device is the Slotted Bolted Connection (SBC), developed at UC Berkeley. The SBC is a modified bolted connection designed to dissipate energy through friction during cyclic tension–compression loading. For example, an SBC can be installed between a brace end and a frame joint in a building structure [20].

Tirca et al. [21] conducted both numerical analyses and full-scale testing of friction braced frames (FBFs) equipped with pall slotted bolted connections (SBCs). Their findings indicated that ductility and overstrength-related force modification factors of 5.0 and 1.1, respectively, are appropriate for buildings up to 10 stories in Canada. In addition to the FBFs, the seismic resistance frame system (SRFS) must incorporate flexible backup moment-resisting frames (MRFs) designed to carry 25% of the seismic forces assigned to the FBFs. The members of these MRFs should be proportioned so that the frame remains essentially elastic under story drifts of up to approximately 1.5% of the story height.

A new friction damper device has been proposed, consisting of three steel plates that rotate relative to each other around a pre-stressed bolt, which holds the plates together. Between these steel plates, two circular friction pad discs provide dry friction lubrication, ensuring a stable frictional resistance during movement. For the analysis, a friction pad disc with a coefficient of 0.4 was considered. Both numerical and experimental studies were conducted under various ground acceleration records. The results indicated that the friction-damped frame maintained satisfactory performance even under seismic events with peak ground accelerations (PGA) 50% higher than the design level, although this was accompanied by significantly larger rotation demands on the friction damper device [22,23].

Rather than relying on external energy-dissipating devices, the concept of a semi-rigid, moment-resisting steel frame based on a weak-joint–strong-column philosophy offers significant advantages over conventional rigid moment resisting steel frames (MRSFs) for both standard design and damage-resistant design. Two suitable semi-rigid joint configurations have been developed: the flange bolted joint (FBJ), which is simple to fabricate and erect but has a relatively low damage threshold, and the sliding hinge joint (SHJ), which is also straightforward to fabricate, slightly more complex to erect, but provides a high damage threshold. Additionally, a partial isolation system applied at each floor level is feasible and provides benefits in terms of enhanced damage resistance under design-level ultimate limit state earthquake loading [24–26].

Latour et al. [27] tested different friction interface materials, including steel-on-steel, brass-on-steel, Friction Material SA-21 (M1, a rubber-based material typically used in electric motor brakes) on steel, and Friction Material STR-396 (M2, a hard rubber material designed for low-wear applications) on steel. The results indicated that the static coefficient of friction for the steel-on-steel interface (0.173) was higher than that of the brass-on-steel interface (0.097). While the steel-on-steel interface exhibited a high friction coefficient, its behavior was unstable, initially showing pronounced hardening followed by rapid softening. The brass-on-steel interface showed a lower friction coefficient but more stable behavior, with notable hardening. Material SA-21 displayed pinching behavior, a low friction coefficient, and rapid degradation. In contrast, STR-396 exhibited a relatively low friction coefficient but demonstrated very stable behavior and high energy dissipation capacity.

Post-tensioned precast concrete frame structures are particularly well-suited for damage control during earthquakes because their primary mode of deformation occurs as gap openings at the interfaces between precast beams and columns, while the precast members themselves experience little to no damage. A friction damper has been developed to exploit these gap-opening displacements, providing supplemental passive energy dissipation to the frame. The dampers function by utilizing the friction generated between adjacent metallic surfaces as the gaps at the beam-to-column interfaces in unbonded post-tensioned precast concrete frames open and close during seismic events [28].

A bolt-prestressed friction mechanism with a frictional interface, consisting of stainless steel and a new non-asbestos organic brake-lining pad, dissipates seismic input energy as the system undergoes lateral deformations. Cyclic tests were conducted to evaluate the efficiency of the proposed friction interface and its performance under seismic loading conditions. The results demonstrated that the frictional behavior is stable, repeatable, and predictable, despite the relatively low friction coefficient of the interface [29].

Wolski et al. [30] recently developed a friction device for special-concentric moment-resisting frames (SC-MRFs), termed the bottom flange friction device (BFFD). This device is attached solely to the beam's bottom flange, avoiding interference with the floor slab and facilitating easy replacement, if necessary, following an earthquake.

Instead of installing friction-dissipating systems at the brace locations or beam flanges, friction energy-dissipating devices can be directly placed at steel column bases. These systems utilize the rocking deformation of a free-standing column as the input deformation for friction sliding plates, which are clamped using post-tensioning bolts. Experimental results indicate that the base connections did not exhibit significant strength degradation, even under drift cycles up to 4%. However, stiffness degradation was observed, particularly in axially loaded specimens oriented along the weak axis. Stiffener plates placed between the column flange tips were not sufficient to prevent column base yielding [31,32].

Since the energy dissipation of friction dampers primarily depends on the friction coefficient between interacting surfaces, several studies have investigated different types of friction pads beyond the mild-steel pads used in earlier designs [33].

More recent studies have explored the use of Bissaloy steel pads [34,35], which demonstrate fairly stable and repeatable hysteretic responses with minimal surface wear. However, Golondrino et al. [34] noted that these materials may produce friction coefficients lower than 0.2 when the tightening torques range between 350 and 500 Nm.

Latour et al. [36] further investigated non-metallic materials, identifying several that exhibit stable hysteretic behavior under uniaxial cyclic displacement histories. These materials have friction coefficients close to 0.2, which are largely independent of both contact pressure and sliding velocity.

Frictional sliding can lead to surface wear, which may result in an unstable force–displacement hysteretic response under cyclic loading. To address this instability, various friction pad materials have been explored, including brass pads. Brass pads exhibit a more stable hysteretic response compared to mild-steel pads; however, galvanic corrosion presents a potential challenge. Further investigations have examined steel plates coated with sprayed aluminum as an alternative [37–39].

This approach can provide a relatively stable force–displacement hysteretic response for the friction device. However, the resulting friction coefficients are somewhat dependent on the contact pressure. Furthermore, the coating process is complex, typically requiring specialized equipment to ensure high-quality control and optimal performance of the coated steel plates and their sliding interfaces. Consequently, the overall cost of such friction pads may be prohibitively high.

Wolff [40] investigated the use of stainless steel plates coated with non-asbestos organic (NAO) materials in base isolation systems. Paronesso and Lignos [41] report 62 experimental tests on five non-metallic friction pads for potential use in seismic friction dampers. Using a full-scale sliding damper prototype, the effects of contact pressure, loading protocol, and loading rate were examined. Two pads exhibited stable static and dynamic friction coefficients of approximately 0.2–0.3, largely independent of pressure, temperature, and loading conditions, provided the sliding velocity exceeded 10 mm/s.

Using low-cycle reciprocating load tests to evaluate their influence on friction damper performance. The results indicate that the brass–steel (S-CO) and titanium–steel (S-T) pairs exhibit hysteretic curves that closely approximate ideal rectangles, characterized by symmetric force–displacement behavior and stable energy dissipation. Among them, S-CO provides the highest energy dissipation (≈18.45 kJ), while S-T (≈10.43 kJ) maintains similarly stable performance. In contrast, the zirconia ceramic–steel (S-CE) pair performs reliably only at small displacements (≤15 mm); at larger displacements, significant friction-force divergence occurs, reducing curve symmetry and overall stability. The friction coefficient between the friction plates and the main plates plays a critical role in damper behavior. Although S-CE exhibits the highest average coefficient (0.518), its friction response is unstable due to oxidative wear of the ceramic surface. In comparison, S-CO (0.399) and S-T (0.213) demonstrate more stable friction coefficients that become consistent with appropriate surface roughness, enabling reliable long-term damper operation [42].

Regarding the performance of the metal friction damper, Cyclic loading tests were performed on 30 specimens to evaluate the effects of loading sequence and loading rate under both high-speed (20–60 mm/s) and low-speed (0.2–3 mm/s) conditions. Five friction-pair configurations were examined: brass–hot-rolled steel with untreated surfaces (B-HS), brass–hot-rolled steel with polished surfaces (B-PHS), brass–stainless steel (B-SS), stainless steel–hot-rolled steel with untreated surfaces (SS-HS), and stainless steel–hot-rolled steel with polished surfaces (SS-PHS). The results indicate that all specimens exhibited full, rigid–plastic hysteresis loops across all loading rates, and their mechanical indices satisfied the variability requirements specified in FEMA-356 [43].

A parametric study of square rotational friction dampers was conducted using finite element analysis, considering variations in the friction coefficient, bolt–washer radius, and initial rotation angle under cyclic

loading. The results indicate that dampers equipped with all three types of friction pads exhibit strong energy dissipation capacity. The sliding force increases with the pretension force applied to the high-strength bolts. Dampers with brass friction pads generate the highest sliding force, whereas those using non-asbestos composite friction pads provide stable performance with comparatively lower friction demand [44].

Brake pad friction dampers are proposed in the bracing location of steel structures. A combined experimental–numerical program was conducted to assess their energy dissipation capacity. Cyclic loading tests were performed to evaluate the behavior of individual damper components, while finite-element analyses in Abaqus and OpenSees examined the performance of these dampers when integrated into knee-braced frames (KBFs) subjected to seismic excitation. The findings demonstrate the potential of brake pad friction dampers to enhance the seismic performance of KBFs, offering an innovative and cost-effective approach to improving earthquake resilience in structural systems [45].

Xu et al. [46] present the development and evaluation of a new metal–friction hybrid damper (MFHD). The device comprises three key components: an elastoplastic module, a friction module, and a stop module organized into a three-stage working mechanism consisting of a friction stage, a coupled stage, and a residual stage. The seismic performance of the MFHD was examined through quasistatic tests conducted on eight specimens. The study evaluates the influence of segment length, segment diameter, and slipping displacement on the mechanical behavior of the damper. The results show that increasing the segment diameter by 15% enhances the stiffness by 23.4% and the cumulative energy dissipation (CED) by 44.4%. In contrast, increasing the segment length by 50% and 100% reduces the CED by 6.4% and 56.7%, respectively.

To enhance the energy dissipation and self-resetting capacity of bridge structures during strong earthquakes, Yang et al. [47] proposed a novel buckling-restrained SMA bar-based friction damper (SFD). The damper consists of buckling-restrained super-elastic SMA bars, friction pads, and a steel frame. The SMA bars provide self-resetting capability, while the friction pads contribute additional energy dissipation, thereby improving the overall seismic performance of the system.

Pall and Pall [48] highlighted several advantages of friction dampers, including:

- Large rectangular hysteresis loops and stable cyclic behavior.
- Performance (frictional force) is largely independent of sliding speed and temperature.
- Energy dissipation is achieved through friction rather than through the yielding of structural elements.
- Relatively small and compact size compared to other types of dampers.
- Simplicity and cost-effectiveness.
- Damage-resistant operation during seismic events.

Etedali et al. [49] stated that the tuned mass damper (TMD) is one of the earliest passive control devices used to enhance the safety of tall structures and improve their performance under environmental dynamic loads. TMDs dissipate a portion of the seismic input energy, with only part of this energy being transferred to the main structure. The friction-tuned mass damper (FTMD) is an innovative device that combines the traditional linear TMD concept with a friction damper mechanism. This hybrid device is still under development for seismic applications.

Nouri et al. [50] demonstrated that integrating arch ring dampers (ARDs) into weak moment-resisting frame (MRF) structures significantly improves seismic performance, reducing yield drift by 33% and increasing stiffness by 2.25 times. In addition, the use of ARDs effectively mitigates residual deformations and helps prevent structural collapse under both Design Basis Earthquake (DBE) and Maximum Considered Earthquake (MCE) hazard levels.

As reported by Xu et al. [51], major earthquakes in recent years in China, Chile, New Zealand, and Japan have caused severe damage to numerous building structures, many of which required extensive repair or

complete reconstruction. Consequently, improving the seismic resilience of building structures has become a major focus of research. Energy dissipation dampers have been proposed for installation at selected locations within structures to enhance damping capacity and dissipate a substantial portion of the seismic energy input. However, a key limitation of conventional dampers is their inability to automatically return to their original position after an earthquake, often resulting in residual deformations and significant economic losses. To overcome this drawback, recent studies have proposed integrating self-centering mechanisms with traditional dampers, thereby providing both energy dissipation and self-centering capabilities. Such self-centering dampers have been demonstrated to effectively reduce residual deformations and mitigate post-earthquake structural damage.

A seismic retrofit device consisting of a steel frame with friction hinges and corner springs was proposed and experimentally evaluated under cyclic loading. The springs provide stiffness and restoring force, while the friction components dissipate energy. The mechanical behavior of the device was analytically formulated and validated against experimental results. The retrofit system was then applied to a case study structure originally designed without seismic considerations, and its seismic response before and after retrofit was evaluated using nonlinear time-history analysis. Performance was assessed in terms of inter-story drift, residual displacement, and energy dissipation. The results confirmed that the retrofit frames effectively dissipate seismic energy and significantly reduce both inter-story drifts and residual displacements [52].

A passive seismic control system combining a friction spring damper (FSD) and a pot bearing (PB) was proposed and compared with conventional isolation systems, including lead rubber bearings (LRB) and Friction Pendulum Systems (FPS). Two benchmark buildings were analyzed using nonlinear time-history analysis, with a validated OpenSees material model developed to capture the self-centering behavior of the FSD. The results showed that the proposed system effectively reduced base shear and interstory drift, performing comparably to FPS and outperforming LRB. Owing to its self-centering capability, the system exhibited significantly lower residual displacements, indicating reduced post-earthquake maintenance requirements [53].

Rotational friction dampers (RFDs) are flexible energy-dissipation devices for seismic response control; however, their basic configuration faces challenges related to performance stability, limited strength, and inaccuracies arising from the assumption of uniform clamping pressure on friction pads. To address these issues, four improvement strategies have been proposed: selecting friction materials with stable properties, increasing the friction coefficient, enhancing the clamping force, and optimizing key structural configurations [54].

A novel parallel double-stage crawler-track-shaped shear damper (PDCSD) was developed using thin-walled steel plates. The device achieves an asynchronized double-stage mechanism through parallel energy dissipation (inner and outer steel plates), restraining (upper and lower plates), and load transfer (outer and inner blockers with initial clearance). Theoretical equations for the skeleton curve and load transfer system were proposed and validated through full-scale seismic and fatigue tests. Refined finite element analyses further revealed the working mechanism and confirmed the theoretical predictions. Finally, a simplified model emphasizing the hysteretic behavior was developed and validated against experimental and numerical results, providing an efficient tool for seismic response control in PDCSD-equipped structures [55].

As reported by Grossi et al. [56], an innovative seismic protection device, the bidirectional rotational friction damper (BRFD), was developed for precast RC structures with weak connections. The BRFD functions simultaneously as a beam-to-column joint and a damper, combining rotational friction mechanisms with movable plate geometry to provide damping in two directions, unlike conventional devices that act unidirectionally. Its friction-based energy dissipation enables the device to withstand multiple seismic events without damage while maintaining its damping performance.

Addala et al. [57] proposed a hybrid passive device combining a viscoelastic damper and a friction damper, operating synergistically through a novel locking mechanism. The device mitigates the limitations of individual dampers and enhances structural performance under multiple vibration levels from wind and seismic events. The dampers are arranged in parallel, exhibiting distinct hysteretic behavior: the viscoelastic damper activates under extreme winds and minor to moderate earthquakes, while both devices engage simultaneously during strong seismic events.

Mustafa et al. [58] evaluated viscoelastic (VE) and rotational friction (RF) dampers for coupled shear wall systems through experiments and numerical simulations. VE dampers effectively controlled high-frequency vibrations, while RF dampers provided stable energy dissipation across displacement amplitudes. Experimental and STERA 3D numerical results showed strong agreement in inter-story drift, base shear, and energy dissipation.

Guo et al. [59] proposed an innovative linear friction damper (LFD) to mitigate seismic damage in continuous girder bridges subjected to near-fault ground motions with velocity pulses. Numerical models developed in OpenSees were analyzed under pulse-type records, and the effects of key LFD parameters were examined. Nonlinear time-history analyses showed that the LFD effectively reduced superstructure–substructure relative displacements and significantly decreased pier seismic responses compared with non-isolated bridges, demonstrating performance comparable to conventional isolation systems.

Liang et al. [60] addressed excessive cumulative longitudinal displacement at girder ends of long-span suspension bridges by proposing a parallel damping scheme combining friction and viscous dampers. Analysis of measured data showed that quasi-static displacement, induced by asymmetric cable deformation under moving loads, dominates cumulative displacement. A continuous friction damper model was adopted to control quasi-static responses, while the parallel friction–viscous system achieved dual control by reducing cumulative operational displacement and peak seismic displacement. Most of the damping devices discussed above are patented and require careful selection from commercially available options. Their designs are not generally open to engineers and fabricators for customization, limiting their use primarily to specialized structures. The objective of this research is to propose a friction damper that can be designed and detailed similarly to ordinary structural elements, allowing flexible application according to the specific needs of a structure.

Yue et al. [61] developed a novel energy-dissipating system, the friction damper parallel composite buckling-restrained Brace (FDBRB), which combines a buckling-restrained brace (BRB) with friction dampers in parallel. The study presents the system's configuration, restoring force model, and constraint ratio formulation. Quasi-static tests on friction damper, BRB, and FDBRB specimens, together with numerical simulations, were conducted to evaluate performance and key parameters, including core constraint (width ratio) and load sharing (load ratio). Results indicate that under minor seismic excitations, energy is mainly dissipated by the friction damper, whereas under stronger seismic events, the BRB yields and continues to dissipate energy, effectively mitigating the overall seismic response.

Wu et al. [62] developed a viscoelastic–friction composite damper (VFCD) to overcome the limitations of conventional dampers and achieve graded energy dissipation. Experiments, finite element analyses, and fatigue tests investigated key factors, including load frequency, viscoelastic cross-section, bolt preload, material thickness, and friction coefficient. Results show that VFCDs combine velocity- and displacement-dependent behavior with multistage energy absorption, and that increasing viscoelastic cross-section, bolt preload, or friction coefficient enhances slip force and energy dissipation.

In this research, a new type of friction damping system is proposed, which combines a leaf spring commonly used in vehicle suspension systems with a rotational sliding core plate mechanism. The behavior of

the rotational core plates is similar to that of conventional rotational friction dampers; however, the inclusion of the leaf spring may alter the overall response of the combined system. Several studies have previously investigated the energy-dissipation characteristics of leaf springs, providing a basis for understanding their contribution to the hybrid system.

Leaf springs consist of flat metal strips shaped into an elliptical arc and appropriately tempered. They are capable of absorbing and releasing energy and are commonly used in vehicle suspension systems.

Friction between the layers of the leaf springs provides additional energy dissipation. The energy is dissipated through the force required to overcome the clamping forces of the leaves and the sliding displacements occurring within the leaf layers.

The principles of friction damping devices are straightforward, and they can be manufactured locally, reducing overall costs. Retrofitting with friction dampers is considerably less expensive compared to conventional approaches. For new steel structures, there is essentially no additional cost if the dampers are locally fabricated and installed. By reducing seismic forces, there is no need for foundation modifications. The damper acts as a fuse element, limiting earthquake forces to the total slip force along the direction of interest. Being a displacement-sensitive device with a nearly constant slip force, the actual slip varies depending on the characteristics of the ground acceleration. This slip controls the inter-story drift, for which the building must possess adequate ductility, even if minimal. The slip forces developed in friction damper will be resisted by additional tension-compression in column/wall.

2 Proposed Friction Damper

2.1 Geometry, Boundary Conditions and Assumptions

The proposed friction damper, shown in Fig. 2, consists of a suspension leaf spring connected to four sets of rotational friction plates assembled using slip-critical bolted connections. The entire system is installed at the corner of a beam–column joint of the frame, as shown in Fig. 3, and is linked through a strut designed to resist the critical buckling forces induced by inter-story drift. The number of friction plates in each set can be increased depending on the required energy dissipation capacity.

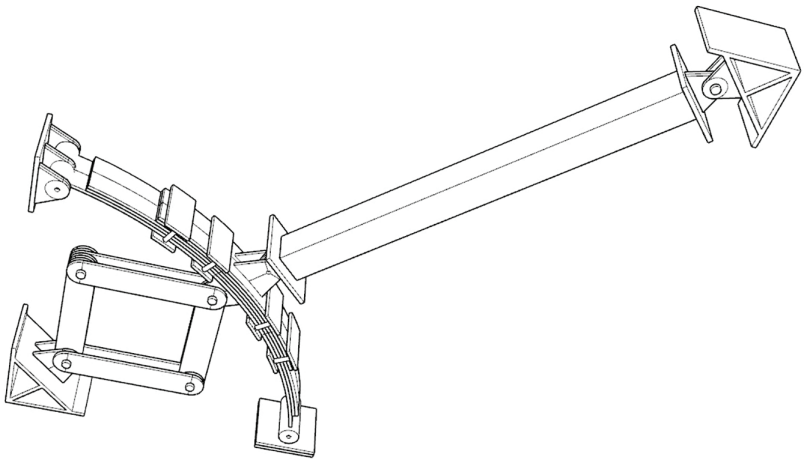

Figure 2: Proposed friction damper setup

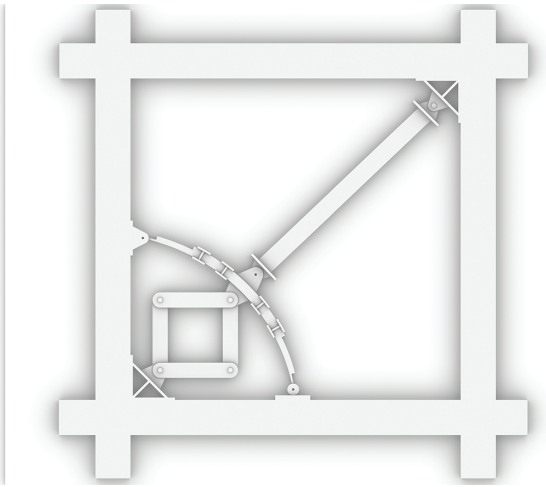

Figure 3: Proposed friction damper in frame

Fig. 4 illustrates the components of the proposed damper with assigned boundary conditions. Anchor Point 1 is connected to the beam–column joint of the frame system. Its geometry may vary when adapting the damper for structures other than buildings, such as bridges or machine foundations. Anchor Point 2 provides the second attachment location and is connected to the buckling-resilient strut through a pinned connection. The lower end of the strut is also pinned to the leaf spring assembly.

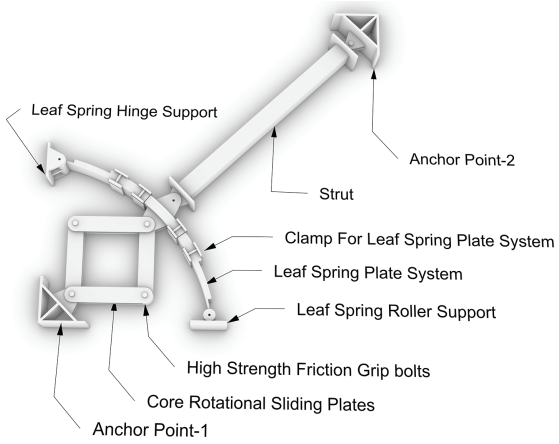

Figure 4: Elements of proposed friction damper system

The leaf springs are clamped together with a specified clamping force to generate normal pressure between the plates, enabling frictional energy dissipation. One end of the leaf spring is connected to the column through a pinned connection, while the other end is connected to the beam via a roller connection to prevent arching in the plates. The combination of hinge and roller connections is intended to minimize unwanted spring effects and ensure that the device behaves predominantly as a damper. In Fig. 4, the upper attachment point of the leaf spring is shown as a hinged connection, while the lower attachment point is detailed as a roller connection that is free to move horizontally.

The span of the leaf spring depends on architectural constraints, such as opening requirements. The maximum permissible length of the core rotational sliding plates is governed by the available space between

the leaf spring and the corner attachment points. The dimensions of the strut should be selected based on its critical compressive capacity relative to the expected damping forces, ensuring that the strut remains effective under both tensile and compressive actions. The inter-story drift component along the strut direction will be the primary driving displacement for the proposed damper.

The width and thickness of the leaf spring plates can be selected so that they remain elastic during energy dissipation, thereby avoiding permanent deformation after cyclic loading. Alternatively, the plates may be designed to allow limited plastic deformation to introduce an additional energy dissipation mechanism through yielding. In this part of the research, the leaf spring plates are considered to perform purely elastically.

A mild steel or brass friction pad can be used as the friction surface between the rotational plates, allowing it to be replaced after the damper experiences a certain level of earthquake loading that may reduce the bolt pretension due to surface wear. To make the system economical, this study proposes the use of a replaceable mild steel friction pad. Determining the earthquake peak ground acceleration (PGA) levels at which the friction pad must be replaced or additional bolt pretension is required will be addressed in a subsequent part of the research.

The leaf spring may consist of a single plate or multiple plates clamped together, where friction between the sliding plates provides additional energy dissipation. The global function of the leaf spring is to restore the damper to its original shape after the cyclic forces cease, while the sliding plates within the leaf spring also contribute to damping. This paper investigates the performance of the proposed damper through theoretical formulation and contact-based nonlinear finite element modelling using ABAQUS. Therefore, this study focuses on the behavior of the damper at the component level, while the structural-level performance of the proposed damping system will be addressed in a subsequent phase of the research.

The equilibrium equations, geometric compatibility conditions, and energy balance principles will be used to derive a simplified formulation of the damper. Appropriate coefficients will be introduced in parts of the derivation where simplified assumptions are applied, and these constants will be calibrated by comparing the analytical results with those obtained from numerical modelling. For implementing this damping system in a frame structure, a pair of anchor points corresponding to the leaf spring must be provided on the beam and column. To capture the displacement demand generated by inter-story drift, the system needs to be anchored at two corners of the bay—similar to diagonal bracing—using a compression strut with pinned connections, as shown in Fig. 3.

2.2 Analysis of the Damper

In a broad sense, the overall analysis of the proposed damper can be categorized into two major steps. First, a theoretical formulation of the damper response under cyclic displacement loading is developed. Second, a numerical model of the same damper is constructed in ABAQUS, incorporating contact nonlinearity, and the two sets of results are compared. In the theoretical formulation, the analysis is divided into simplified stages to capture the full response of the damper. The first stage involves developing the theoretical model for the core sliding friction plate system under cyclic displacement loading. This is followed by formulating the combined effects of the core rotational plates and the leaf spring, considering: (i) behavior prior to friction mobilization between the leaf plates, (ii) behavior after friction mobilization of the leaf plates, and (iii) the combined response of leaf-plate friction mobilization and rotational plate sliding. These stages are formulated to compute the total strut force and corresponding strut displacement at each phase of the cyclic loading history.

The resulting closed-form expressions are then implemented in Python to evaluate the damper response for different friction coefficients (0.2, 0.3, and 0.5) and displacement amplitudes of 25, 50, 75, and 100 mm.

The theoretical results are then plotted and compared with those obtained from the contact–nonlinear numerical model.

3 Formulation for Core Part of Friction Damper

3.1 Cyclic Loading Formulation

For formulating the cyclic loading behaviour of the core rotational sliding plates with bolt pretension $\boldsymbol{P}$ (Fig. 5), a small differential element with differential pretension force $\mathbf{d}\boldsymbol{p}$ and differential area $\mathbf{d}\boldsymbol{A}$ is considered, as illustrated in Figs. 6 and 7. The differential torque $\mathbf{d}\boldsymbol{\tau}$ required to mobilize friction is evaluated, and the total torque needed to activate the frictional resistance is obtained by integrating the differential torque over the entire contact area.

Figure 5: Core plate system with bolt pretension force P

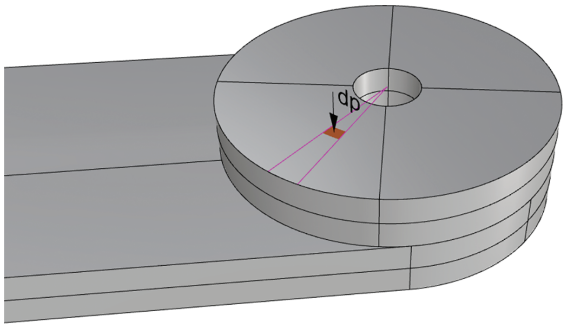

Figure 6: Contact differential element with differential contact prestressing

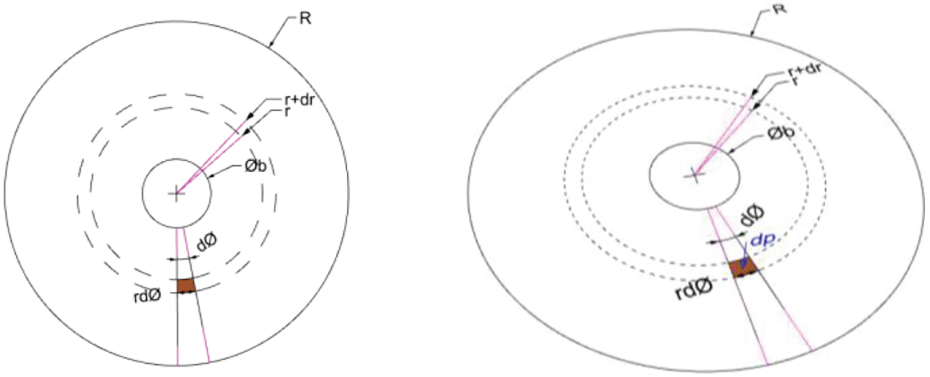

Figure 7: Contact surface elaborated

$P = Bolt\ pretension$

$\mathrm{d}p = pressure\ on\ elemental\ contact\ area\ dA$

$\mathrm{d}A = area\ of\ element = r\mathrm{d}\phi\,\mathrm{d}r$

$\mu = Static\ friction\ coefficient$

Normal reaction in elemental area, $\mathrm{d}R = \dfrac{P}{\pi(R^2 - \phi_b^2)}\mathrm{d}A$.

Corresponding frictional resistance, $\mathrm{d}f = \mu \mathrm{d}R$.

Torque corresponding to the elemental frictional resistance, $\mathrm{d}t = r\mathrm{d}f = r\mu\mathrm{d}R = r\mu\dfrac{P}{\pi(R^2 - \phi_b^2)}\mathrm{d}A$.

$$\mathrm{d}t = r\mu\frac{P}{\pi(R^2 - \phi_b^2)}r\mathrm{d}\phi\mathrm{d}r = r^2\mu\frac{P}{\pi(R^2 - \phi_b^2)}\mathrm{d}\phi\mathrm{d}r \tag{1}$$

Total torque, T Due to all elements ring from radius equal to bolt hole-radius, ϕ_b to Radius of contact disk, R can be evaluated by double integral corresponding to the whole circle and from radius ϕ_b to R,

$$T = \int_{\phi_b}^{R}\int_{0}^{2\pi} r^2\mu\frac{P}{\pi(R^2 - \phi_b^2)}\mathrm{d}\phi\mathrm{d}r = \frac{\mu 2P\left(R^3 - \phi_b^3\right)}{3\left(R^2 - \phi_b^2\right)} = \mu\frac{2PR_e}{3} \tag{2}$$

where, $Re = \frac{\left(R^3 - \phi_b^3\right)}{\left(R^2 - \phi_b^2\right)}$, which represents the effective radius of the contact disc considering loss due to bolt hole.

T indicates Torque due to frictional resistance is independent of the Contact area and it is equivalent to torque produced by linear frictional force μP acting at a distance $\frac{2PR_e}{3}$ from center of the bolt. Above formulation is for single contact area, if there will be n nos of contact surface per node then the tension at that node will be

$$T = n\mu\frac{2PR_e}{3} \tag{3}$$

For 4 nos of node in core rotational sliding plates, Total torque due to interacting surfaces will be

$$T = 4n\mu\frac{2PR_e}{3} \tag{4}$$

Differential Work done by this torque for the rotation of core plate system by $\mathrm{d}\theta$,

$$\mathrm{d}W = T\mathrm{d}\theta = 4n\mu\frac{2PR_e}{3}\mathrm{d}\theta \tag{5}$$

The history of $\mathrm{d}W$ will give all such differential work done corresponding to $\mathrm{d}\theta$,

The assumed coordinate system is shown in Fig. 8. For the core sliding system with bolt centre-to-centre distance L along the arm (Fig. 9), let the initial undeformed diagonal length be $OA = g$. The relationship between the diagonal length g and the angle between rotational plates ϕ is obtained by solving triangle OAB in Fig. 9:

$$\cos\phi = \frac{\left(L^2 + L^2 - g^2\right)}{2L^2} = 1 - \frac{g^2}{2L^2},\ \sin\phi = \frac{g}{L}\sqrt{\left(1 - \frac{g^2}{4L^2}\right)} \tag{6}$$

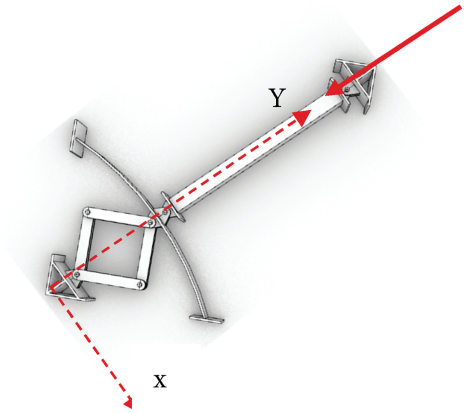

Figure 8: Core plate, leaf spring and strut system

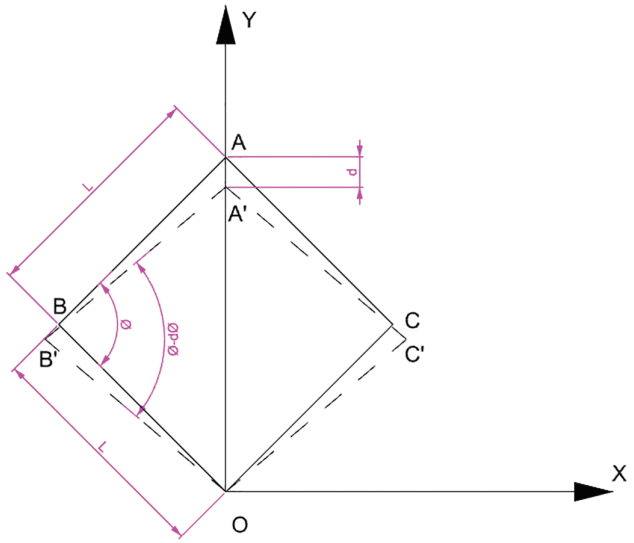

Figure 9: Core plate centerline, changing shape with strut displacement

Differentiating both sides with respect to ϕ:

$$\sin\phi = \frac{g}{L^2}\frac{\mathrm{d}g}{\mathrm{d}\phi}$$

$$\mathrm{d}\phi = \frac{g}{L^2\sin\phi}\mathrm{d}g$$

$$\frac{\mathrm{d}g}{\mathrm{d}\phi} = \frac{L^2\sin\phi}{g} \tag{7}$$

Now the differential work done becomes,

$$\mathrm{d}W = T\mathrm{d}\phi = 4n\mu\frac{2PR_e}{3}\frac{g}{L^2\sin\phi}\mathrm{d}g \tag{8}$$

This equation can be used to evaluate the frictional energy dissipation by the core sliding plate system.

This is the internal energy dissipation, equating this to external energy.

$$Fc\mathrm{d}g = \mathrm{d}W$$

$$Fc = \frac{\mathrm{d}W}{\mathrm{d}g} = 4n\mu\frac{2PR_e}{3}\frac{g}{L^2\sin\phi} = 4n\mu\frac{2PR_e}{3}\frac{1}{L\sqrt{\left(1-\frac{g^2}{4L^2}\right)}} \tag{9}$$

Above relationship between Strut Force and diagonal length of core can be used to plot Strut force vs. strut displacement. g being the diagonal length of core geometry will be always greater than the L As initial angle between core arm plate is 90, the length of the diagonal will be, $g = \sqrt{2}L$. Practically $g = 2L$ is not possible to make Eq. (9) singular.

If dg is -ve, Fc will be compressive, If dg is +ve, Fc will be tensile, from point where tensile force changes to compression force.

In general case,

$$Fc = 4n\mu\frac{2PR_e}{3}\frac{1}{L\sqrt{\left(1-\frac{g^2}{4L^2}\right)}}$$

$$Fc = 0,\ if\ velocity,\ v = 0$$

$$Fc = 0,\ if\ velocity,\ v = 0$$

Internal compressive force developed in core plates just before to the friction mobilization,

$$C = \frac{Fc}{2\cos\phi/2} \tag{10}$$

Total Internal Energy stored $Ein = \frac{4CL}{btE}$.

External work done $Eext = Fc\delta$.

This gives vertical deflection, δ corresponding to frictional mobilization at any stages of loading where for stick to slip condition,

$$\delta = \frac{2L}{btEcos\phi/2} \tag{11}$$

Stiffness corresponding to the core plate system just before slip starts,

$$Ec = \frac{FcbtE\cos\phi/2}{2L} \tag{12}$$

Fig. 10, illustrates the geometric parameters of the core rotational plate system, where L and b denote the length and breadth of the rotational plate, respectively. The parameter g represents the diagonal length of the undeformed core plate system and varies with the strut displacement under cyclic loading. These parameters are assumed for sample calculations to develop the hysteretic response of the core sliding plates, as shown below.

For, L = 600 mm

Initial Diagonal Length, g = 848.528 mm

Nos of Contact surface, n = 2 per node

Width of the core plate, b = 130 mm

Radius of contact disk, R = b/2 = 65 mm

Coefficient of sliding friction between plates, μ = 0.5, 0.3, 0.2

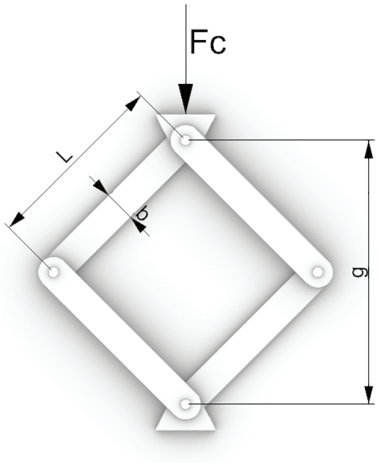

Figure 10: Core plate system dimensions

The coefficient of friction is assumed to take parametric values of 0.5, 0.3, and 0.2. The realistic friction coefficient must be obtained experimentally in order to determine the actual damper forces. Using the above-derived formulation, hysteretic curves corresponding to strut peak displacements of 100, 75, 50, and 25 mm are evaluated and presented in Figs. 11–13 for the different friction coefficients.

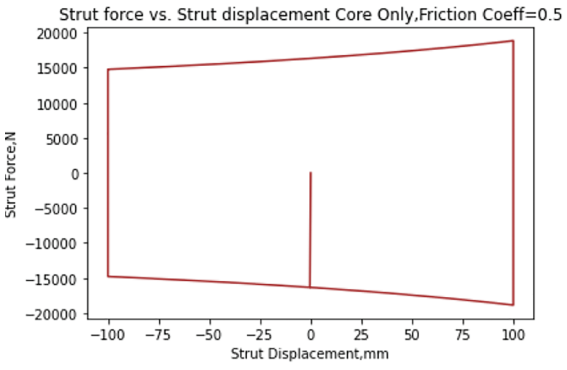

Max Strut Displacement = 100 mm

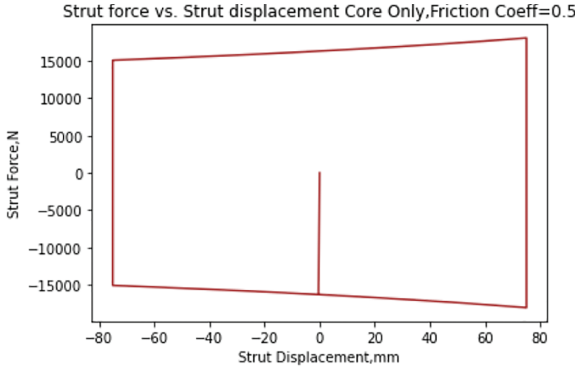

Max Strut Displacement = 75 mm

Figure 11: (Continued)

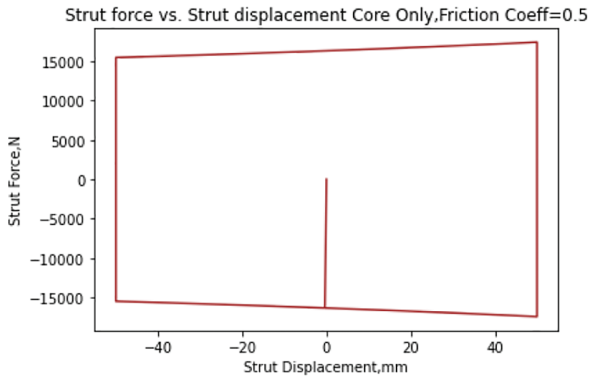

Max Strut Displacement = 50 mm

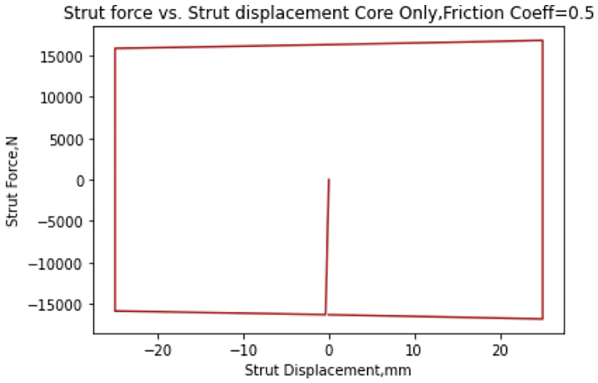

Max Strut Displacement = 25 mm

Figure 11: For Static friction coefficient = 0.5, Hysteretic diagram of central rotational plate system only for strut displacement of 100, 75, 50 and 25 mm

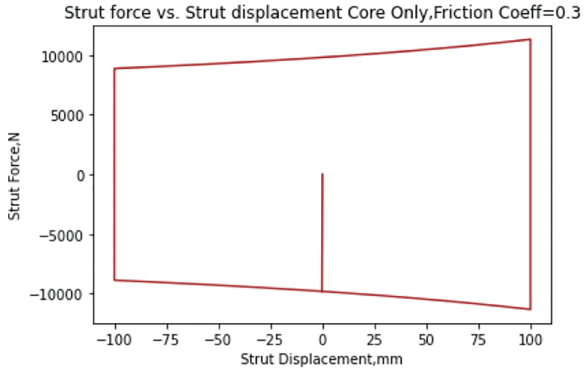

Max Strut displacement = 100 mm

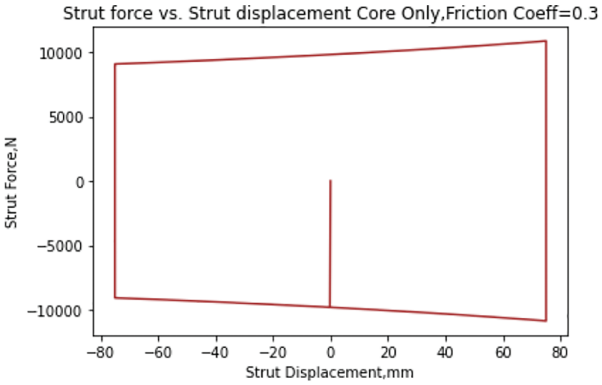

Max strut displacement = 75 mm

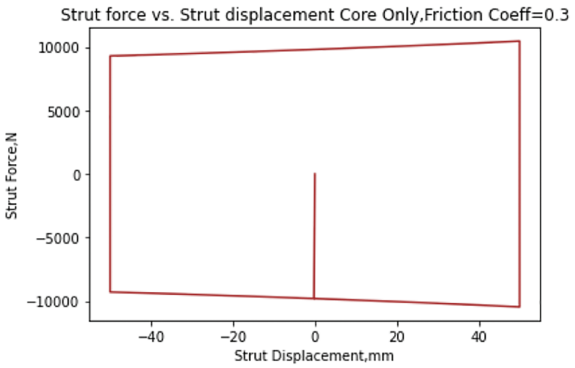

Max strut displacement = 50 mm

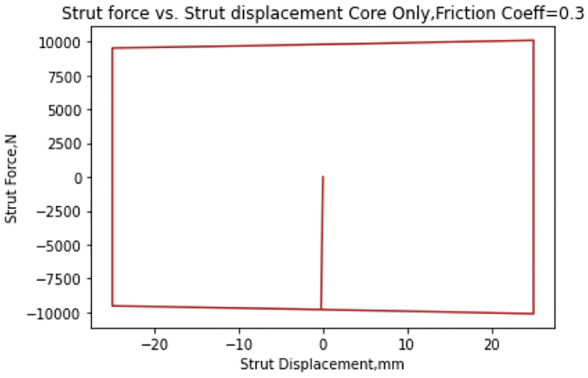

Max strut displacement = 25 mm

Figure 12: For Static friction coefficient = 0.3, Hysteretic diagram of central rotational plate system only for strut displacement of 100, 75, 50 mm

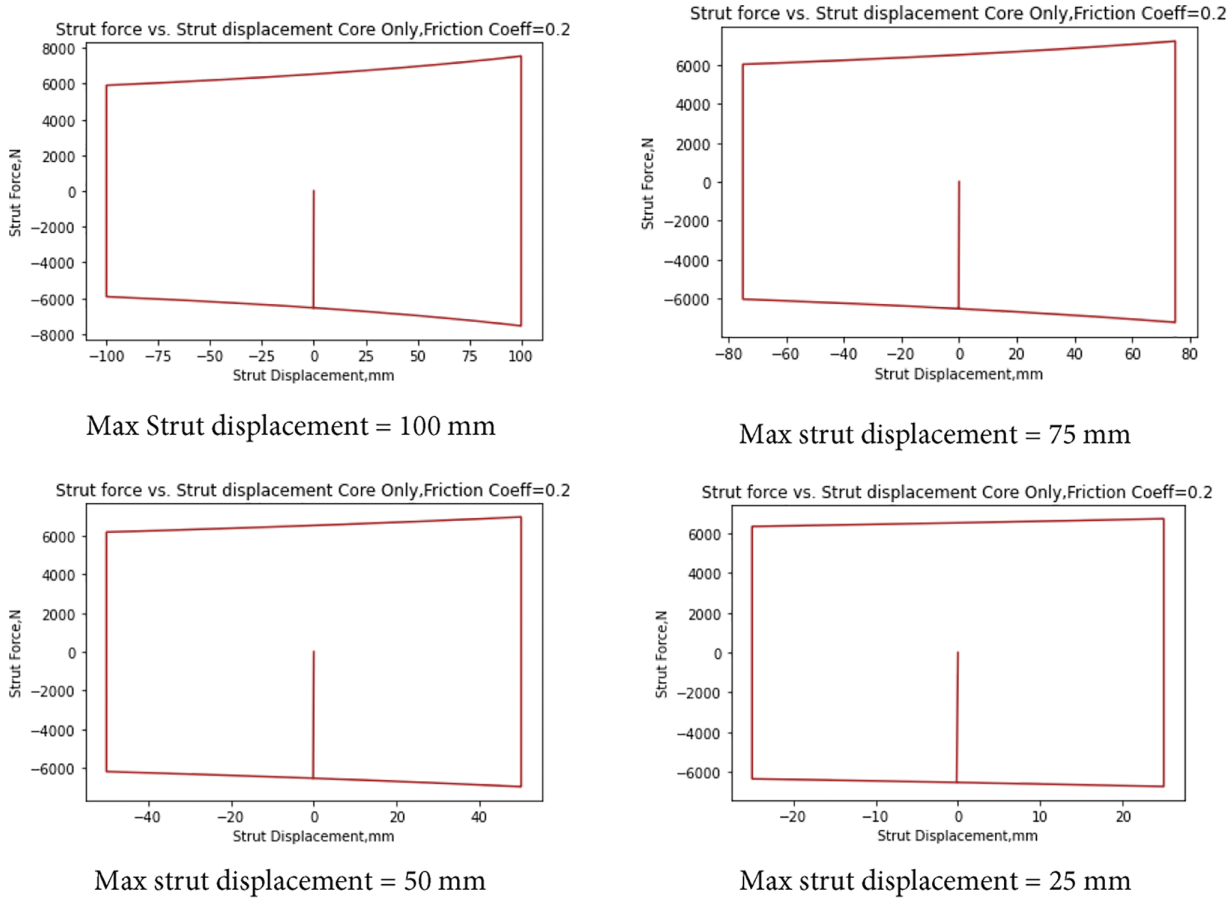

Figure 13: For Static friction coefficient = 0.2, Hysteretic diagram of central rotational plate system only for strut displacement of 100, 75, 50 and 25 mm

From Figs. 11–13, it can be observed that as the friction coefficient increases, the energy dissipation (represented by the area of the hysteretic loop) also increases. The increase in energy dissipation is approximately proportional to the increase in the static friction coefficient.

3.2 Formulation of Sliding Core Plate System with Outer Suspension Leaf Spring

As shown in Fig. 14a,b, a leaf-spring system consisting of plates clamped with a specified clamping force (CF), with one end hinged and the other supported by a roller, exhibits overall behavior equivalent to that of a centrally loaded simply supported beam, as illustrated in Fig. 14c. The clamping force prevents relative slip between the leaf plates until the inter-plate friction is exceeded.

Prior to slip, the assembly of leaf plates behaves as a single composite beam. The central force required to induce a vertical displacement equal to the top-node displacement of the core system, d, can be expressed analogously to the maximum deflection of a simply supported beam subjected to a central point load, F_s, as shown in Fig. 14c.

Once this frictional limit is surpassed, the plates behave as individual beams sliding over one another. The maximum frictional resistance between the leaf plates is comparable to the interface shear developed due to beam bending.

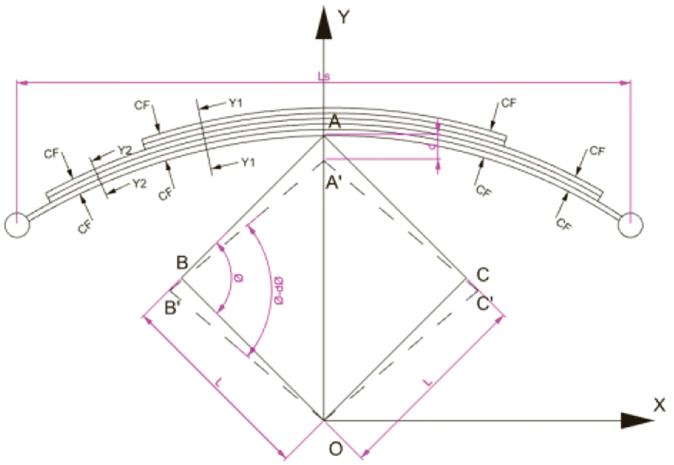

(**a**)**:** Leaf spring and core sliding plate system parameters

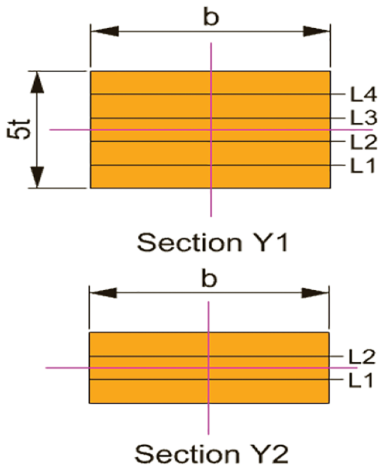

(**b**)**:** Leaf spring cross sections

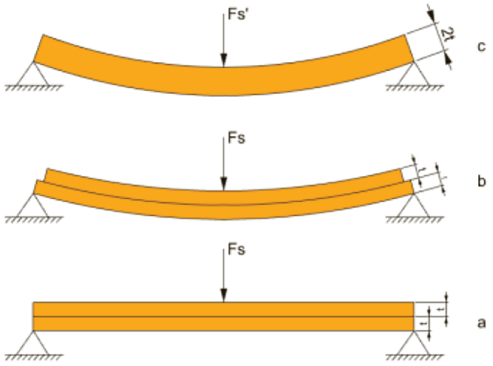

(**c**)**:** Deflection of leaf spring beam analogy vs. deflection of ordinarybeam under central point loading.

Figure 14: Beam analogy corresponding to leaf spring

Fig. 15a shows the vertical shear stress in one of the leaf-plate elements. Fig. 15b presents an enlarged view of the leaf-plate element illustrating the vertical shear stress and the corresponding cross-shear stress. Fig. 15c depicts the overall distribution of bending stress as well as shear stress in the leaf-spring cross-section prior to slip between the leaf-spring plates.

$$Fs = \frac{48EI}{dLs^3} \tag{13}$$

The Force Fs is limited to the force corresponding to which leaf spring plates starts sliding.

Shear stress at distance y from neutral axis,

$$\tau = \frac{Fs}{2Ib} \int y \mathrm{d}A \tag{14}$$

Vertical Shear force at any section: $Fs/2$.

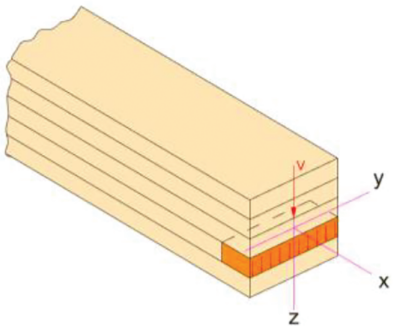

(**a**): Vertical shear stress in leaf spring plate elements

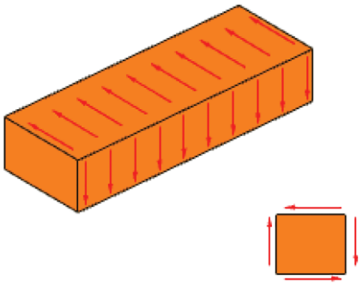

(**b**): Enlarged view of elements showing vertical and cross shear stress in leaf spring plate elements of Fig. 15a

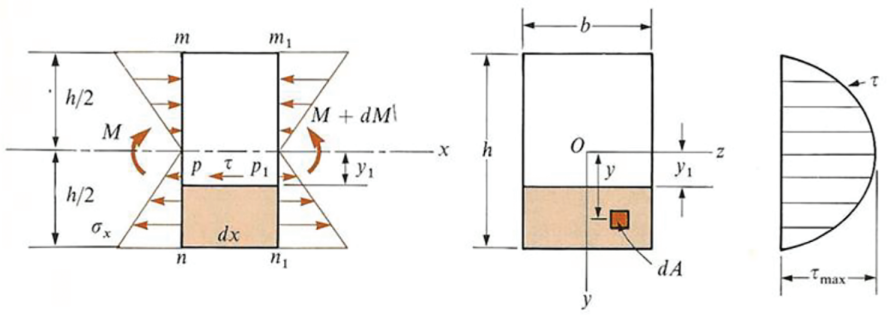

(**c**): Bending stresses and shear stress distribution in leaf spring cross sections before sliding in-between

Figure 15: Stress distribution in leaf spring cross section before slip

First moment of area below interested layer where shear stress need to be evaluated $\int y\mathrm{d}A$, Since there is no any other forces than central force in leaf spring system, shear force at any section is $Fs/2$.

The minimum shear stress is in between outer interfering layer as suggested by shear stress distribution diagram.

If we expect sliding between interface of leaves, we need to apply clamp force equal to minimum out of all layers of shear.

Corresponding shear stress will be shear stress between outermost contact surface.

For n nos of layer of leaf at central zone:

Moment of Inertia, $I = \frac{bh^3}{12}$, $h = nt$, $n = no$ of leaves at considered section.

First moment of area on outermost contact surface,

$$\int y\mathrm{d}A = \frac{(n-1)\,t}{2}bt \tag{15}$$

Corresponding shear stress,

$$\tau = \frac{3Fs}{bh^3}(n-1)\,t^2 \tag{16}$$

Total shear force corresponding to this shear for the contact area bL,

$$SF = \frac{3FsL}{h^3}(n-1)\,t^2 \tag{17}$$

For no of clamp bolt of N, the minimum amount of clamp force required will be,

$$CF = \frac{SF}{\mu N}$$

$$SF = CF\mu\mathrm{N}$$

$$Fs = \frac{SFh^3}{3L(n-1)\,t^2} = \frac{CF\mu Nh^3}{3L(n-1)\,t^2} \tag{18}$$

Deflection in leaf spring system due to this central loading,

$$\delta = \frac{FsLs^3}{48EI} = \mathrm{d}g \tag{19}$$

This deflection should be equal to the change in diagonal length of the core rotational sliding plates of the system dg, After slip between forces the further deflection in plate will be resisted by individual leaf plates. The thickness of leaf plates need to be selected so that the leaf plates will be with in elastic limit for the displacement range corresponding to strut displacement.

Additional resisting force developed due to individual beam action of leaf plates after slip, Fl.

$$Fl = \frac{48EnI}{Ls^3}abs(go-g) = \frac{4Enbt^3}{Ls^3}abs(go-g) \tag{20}$$

$$F = Fc + Fs + Fl = Total\ force\ from\ leaf + core,\ combined\ action$$

$$F = 4n\mu\frac{2PR_e}{3}\frac{1}{L\sqrt{\left(1-\frac{g^2}{4L^2}\right)}} + \frac{CF\mu Nh^3}{3L(n-1)\,t^2} + \frac{4Enbt^3}{Ls^3}abs(go-g) \tag{21}$$

For $g = go + \Delta g\ or\ go - \Delta g$, $F = F$ max.

Area of hysteretic Loop $ED = F\,\mathrm{max} \times 2\Delta g$.

The more precise relation can be obtained by experimental verification and evaluating the correction coefficients Corresponding to leaf spring slip force α and leaf spring force after slip β.

$$F = 4n\mu\frac{2PR_e}{3}\frac{1}{L\sqrt{\left(1-\frac{g^2}{4L^2}\right)}} + \alpha\frac{CF\mu Nh^3}{3L(n-1)\,t^2} + \beta\frac{4Enbt^3}{Ls^3}abs(go-g) \tag{22}$$

Eq. (22) with $\alpha = 1$ and $\beta = 1$ is used to plot the force, F vs. Cyclic Strut displacement for peak displacement of 25, 50, 75 and 100 mm is shown in Fig. 16.

Because a simplified friction model is assumed for the interfaces between the leaf springs and the rotational plates, some discrepancies can be observed between the hysteretic curves obtained from the theoretical formulation and those from the numerical model. These discrepancies can be reduced by adjusting the parameters α and β. Determining these values remains a subject for future research.

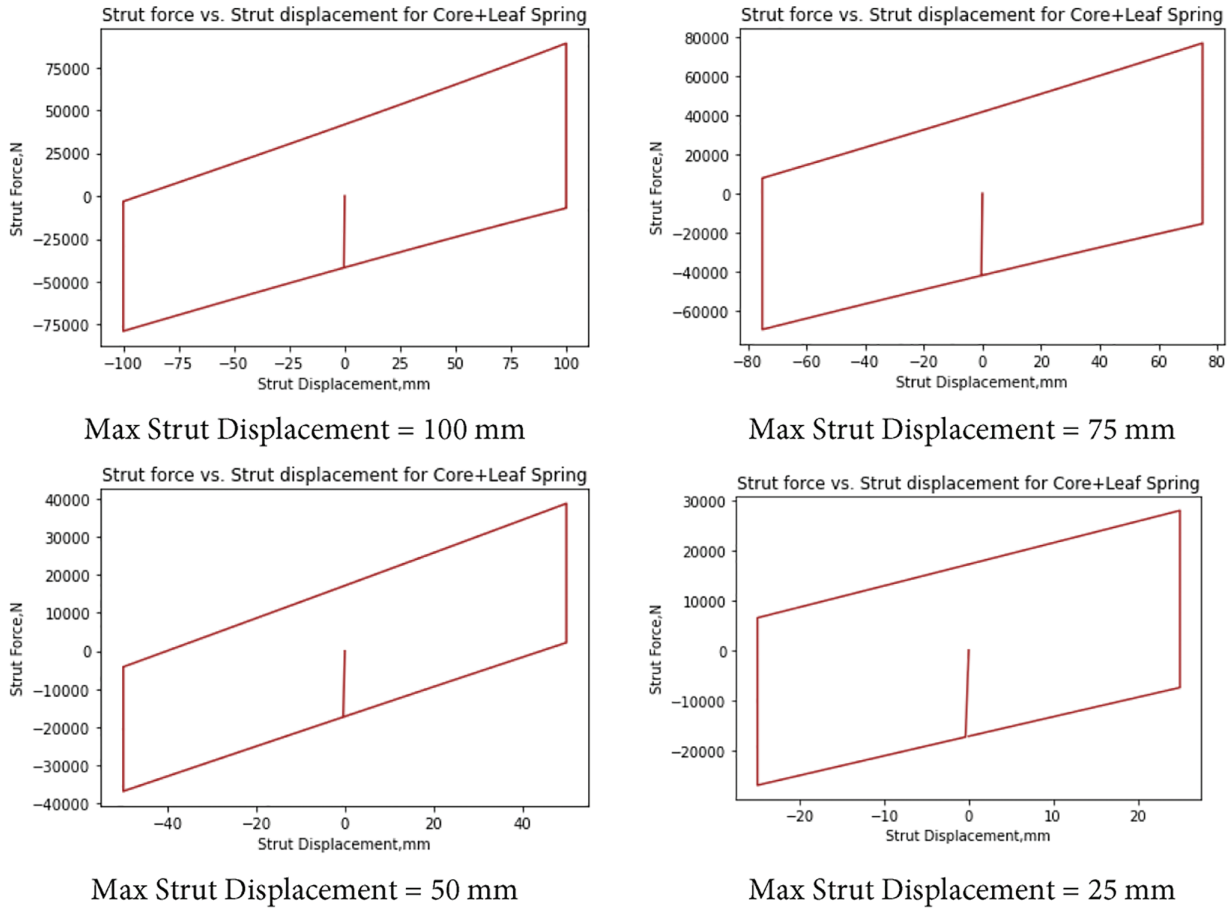

Figure 16: For Static frictional coefficients = 0.5, Hysteretic diagram of central rotational plate + Leaf Spring system for strut displacement of 100, 75, 50, and 25 mm

4 Comparison with Numerical Modeling Force Deformation Output

4.1 Numerical Modelling of Core Sliding Plates

Fig. 17 shows the core rotational plate system modeled in ABAQUS using C3D8 eight-noded brick elements with 2 × 2 × 2 Gauss integration points. A nonlinear quasi-static analysis incorporating contact nonlinearity was performed. The contact interfaces between the rotational plates and friction pads were modeled using Coulomb friction. For the contact nonlinearity model, a penalty-based tangential contact formulation with a friction coefficient of 0.5 was adopted, while hard contact was defined in the normal direction. A surface-to-surface contact formulation was used throughout the analysis. Bolt pretension was applied incrementally in steps of 10% over a duration of 1 s, followed by cyclic displacement loading with a maximum amplitude of 25 mm applied from 1 to 7 s.

Fig. 18 illustrates the applied cyclic displacement history with a peak value of 25 mm. The loading duration was selected to be sufficiently long to avoid inertial effects, ensuring that the response remained quasi-static rather than dynamic.

Fig. 19. shows hysteretic curve plot corresponding to Strut forces vs. cyclic displacement loading. The area enclosed by the hysteretic curve is the energy loss per cycle of the displacement loading. This numerical model output has been compared with the theoretical formulated model and shown in Fig. 20.

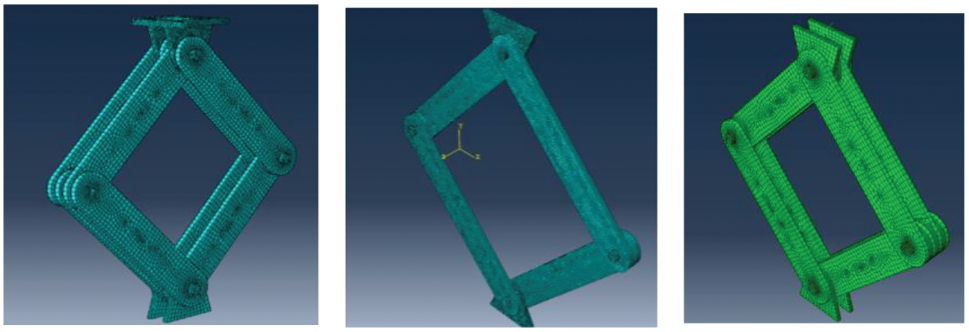

Figure 17: Rotational plate system only numerical model in abaqus

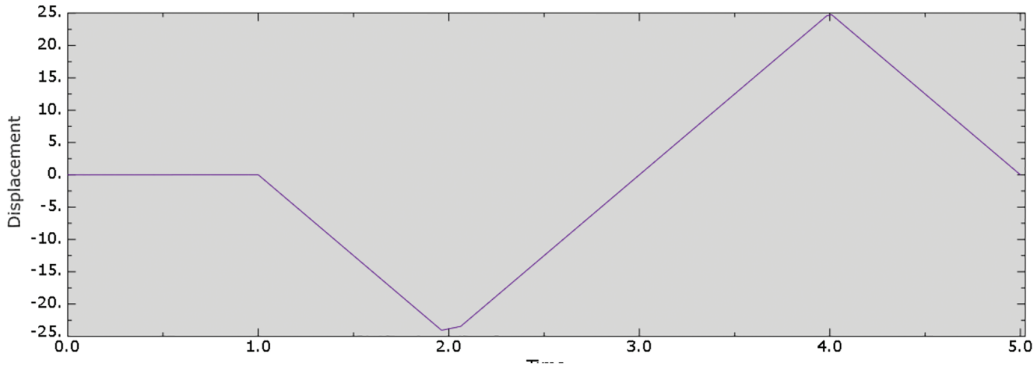

Figure 18: Displacement loading applied to the core plate system: Up to 1 s. bolt pre-tensioning from 1 to 7 s cyclic displacement loading with max displacement of 25 mm

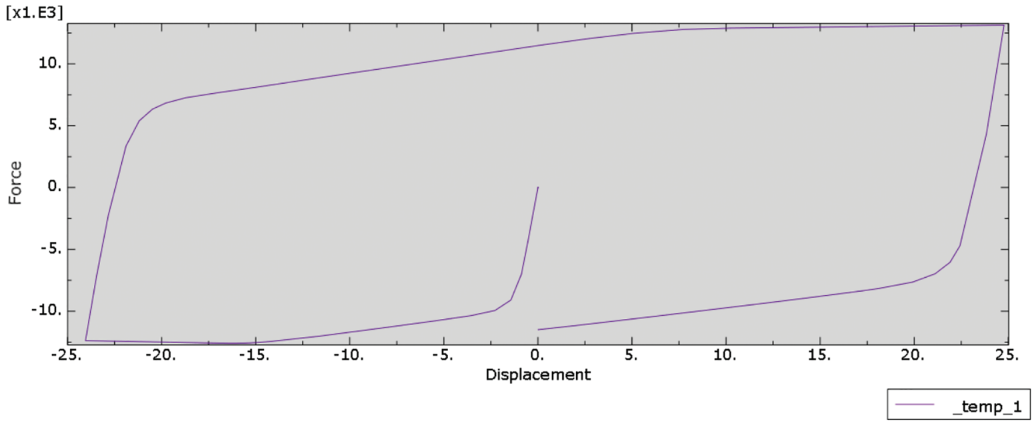

Figure 19: Hysteretic response for 25 mm cyclic displacement for core rotational plate system only

The theoretically formulated hysteretic curve approximately fits the numerical model output with slightly overestimation in the energy loss per cycle due to the simplified friction model used during formulation. Although this discrepancies, it is close enough for the structural uses.

4.2 Numerical Modelling of Core Sliding Plates Cum Leaf Spring: Whole Damper Model

The additional leaf plates are added to the core friction sliding plates. Leaf plates are proposed to be clamped at some points with suitable clamping forces. The one end of the leaf spring plates is restrained

with a hinged boundary condition and the other end is restrained with roller connection to avoid stiffness corresponding to arching action.

Fig. 21 shows the numerical model of the Leaf Spring Rotational Plate (LSRP) Damper developed in ABAQUS. The leaf spring plates are also modeled using C3D8 eight-noded brick elements with 2 × 2 × 2 Gauss integration points, similar to the core rotational plates. The contact surface between leaf plates is modelled with coulomb friction contact nonlinearity. For the Contact nonlinearity model, the tangential contact: Penalty with friction coefficient 0.5 for model and Hard contact is considered along the normal direction of the contact surface. The surface to surface contact model is considered for analysis. The clamp force is applied as a bolt pre-tension to develop frictional resistance between leaf plates.

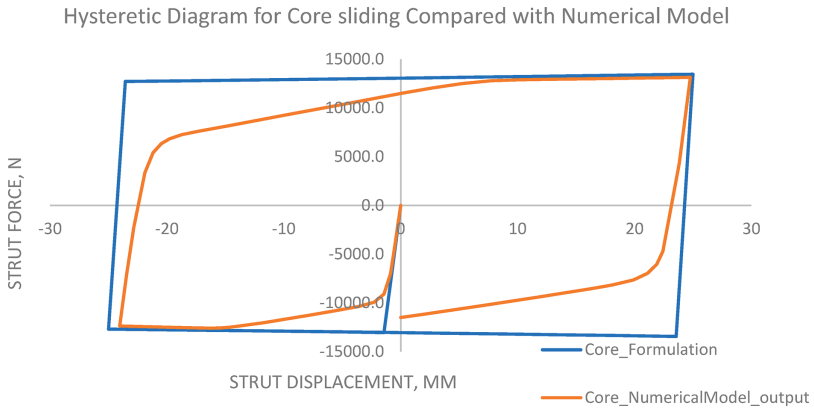

Figure 20: Comparison of hysteretic response from formulation and numerical model output

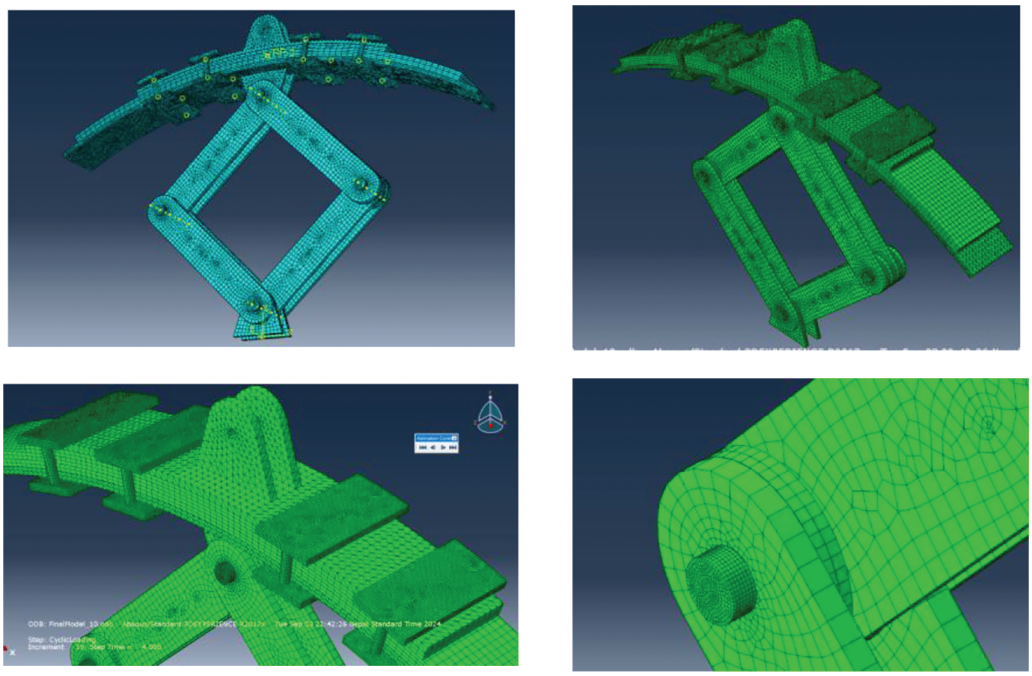

Figure 21: Numerical modelling of core rotational plate cum leaf spring damper system with clamp plates of leaf spring

Up to 1 s period bolt pre-tensioning is applied gradually with 10% of the increments and cyclic displacement loading is applied with maximum displacement of 25 mm from 1 to 7 s period. The analysis is a nonlinear quasi static analysis with contact nonlinearity. Fig. 22 shows the hysteretic response for 25 mm cyclic displacement loading as a numerical model output.

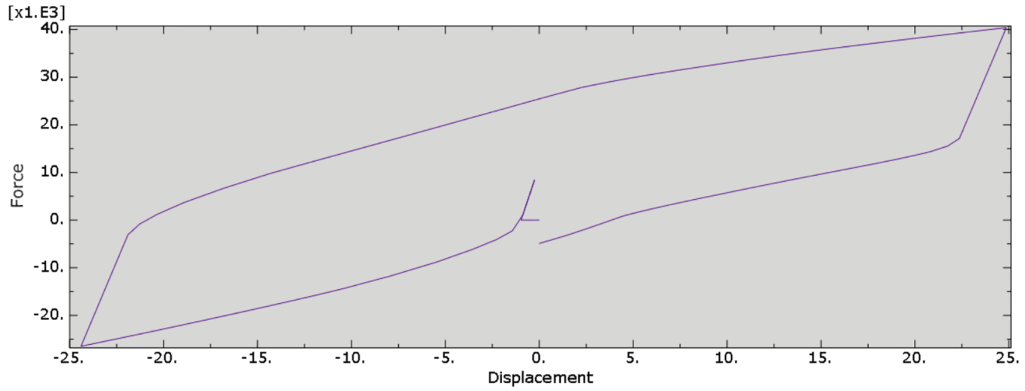

Figure 22: Hysteretic response for 25 mm cyclic displacement for Core+ Leaf Spring system

4.3 Comparison of Hysteretic Force Displacement Response from Numerical Model and Formulation

The comparison in Fig. 23 shows that the hysteretic curves obtained from the theoretical formulation and the numerical model are broadly similar, with only minor discrepancies that can be reduced by adjusting the parameters α and β in the theoretical model. The assumptions used in developing the friction model were intentionally simplified to achieve deterministic results. Nevertheless, this simplified formulation is able to capture hysteretic behavior that closely matches the results obtained from a more rigorous contact–nonlinear numerical model.

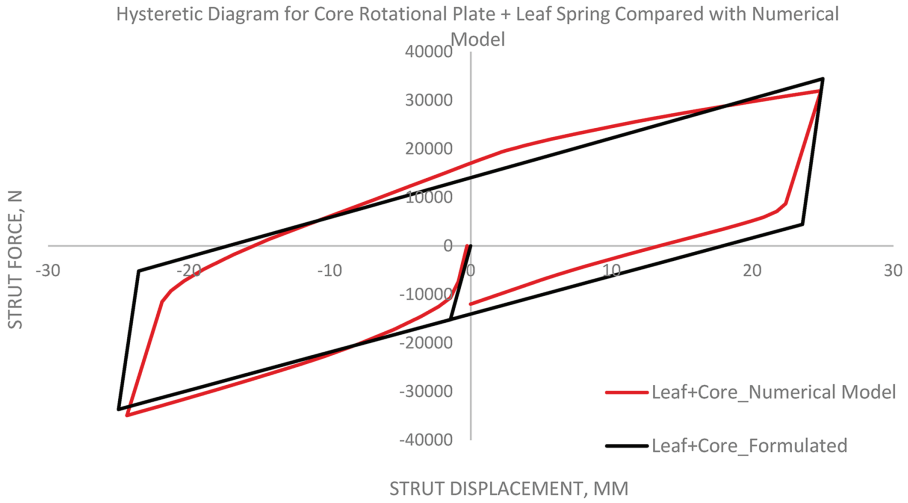

Figure 23: Numerical modelling of core rotational plate cum leaf spring damper system with clamp plates of leaf spring for $\alpha = 1$ $\beta = 1$ (Without applying correction factors in theoretical formulations) For 2 nos of contact surfaces in core rotational plates

5 Equivalent Viscous Damping Ratio

As per the simplified approach proposed by Jacobsen [63], when the damper is applied to the single degree of freedom and at excited with sinusoidal force and at resonance condition when the natural frequency of the system is equal to the forcing frequency, the equivalent viscus damping ratio in terms of area of hysteretic loop i.e., Dissipated Energy, *ED* and Stored Energy *ES*0.

$$\zeta eq = \frac{1}{4\pi}\frac{ED}{ES0} \tag{23}$$

Fig. 24. shows the hysteretic curve, indicating the maximum strut displacement (Δ max), the maximum strut force (F max), and the force corresponding to the onset of slip (Fy). The Energy dissipation value ED is the area enclosed by the hysteretic loop. The approximate value of *ED* can be written as

$$\text{ED} = 2Fy \times 2\Delta \text{ max} \tag{24}$$

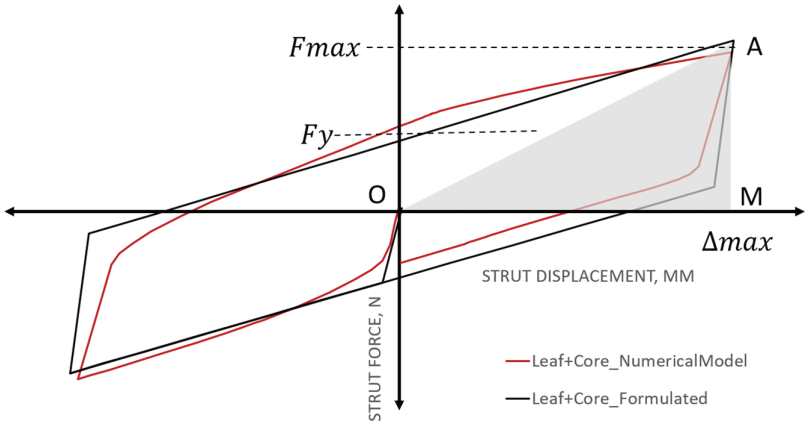

Figure 24: Hysteretic curve parameters

ES0 = The Energy stored is equal to the area enclosed by the triangle, AOM

$$ES0 = \frac{1}{2}F\,\text{max}\,X\Delta\text{max} = \frac{1}{2}k\Delta\text{max}^2 \tag{25}$$

Slope of the line OA = $k = \dfrac{F\,\text{max}}{\Delta\,\text{max}}$.

Equivalent viscos damping ratio becomes

$$\zeta eq = \frac{2}{\pi}\frac{Fy}{F\,\text{max}} \tag{26}$$

The value of Δ max is equal to the maximum strut displacement and in terms of diagonal length of the core plate it will be equal to $abs\,(go - g)$ where go is the initial diagonal length of core rotational plate system and g.

Is the diagonal length corresponding to max strut displacement. These values of g can be used in Eq. (21) to get the maximum strut force,

$$F\max = 4n\mu\frac{2PR_e}{3}\frac{1}{L\sqrt{\left(1-\frac{g^2}{4L^2}\right)}}+\frac{CF\mu Nh^3}{3L\left(n-1\right)t^2}+\frac{4Enbt^3}{Ls^3}abs\left(go-g\right) \tag{27}$$

when $g = go$, the value of strut force will be Fy.

$$Fy = 4n\mu\frac{2PR_e}{3}\frac{1}{L\sqrt{\left(1-\frac{go^2}{4L^2}\right)}}+\frac{CF\mu Nh^3}{3L\left(n-1\right)t^2} \tag{28}$$

These values of Fmax and Fy can be used to evaluate the equivalent viscous damping ratio from Eq. (26).

$$\zeta eq = \frac{2}{\pi}\frac{Fy}{\text{Fmax}}$$

The equivalent viscous damping ratio ζ_{eq} and the damping stiffness k obtained from this formulation can be used directly as damping parameters in numerical models of building structures, without the need to explicitly model the damper. This allows for a rapid assessment of the effectiveness of the selected damper.

6 Losses of Bolt Pretension

Bolt pretension is achieved by applying torque to the bolt head, which induces bolt elongation corresponding to the required pretension force. During cyclic loading and unloading, wear of the friction pad surface may occur, leading to a reduction in pad thickness. This reduction relaxes the bolt's axial deformation by an amount equal to the wear depth. The axial force needed to re-elongate the bolt by this same amount corresponds to the loss of pretension. Therefore, monitoring the overall thickness of the rotational plate assembly (i.e., the combined thickness of the rotational plates and friction pad) can indicate both the need for re-tensioning and the approximate amount of additional pretension required. This can be achieved using two simplified approaches:

(a) **Monitoring component stack depth:** By measuring the total depth of the components between the bolt head and nut, any reduction in length can be directly related to pretension loss. The same amount of additional pretension can then be reapplied.

(b) **Marking bolt-nut alignment:** By marking the relative alignment of the nut and bolt head after initial pre-tensioning, any relaxation of the bolt due to pad wear will cause a rotation of these marks. The change in orientation is directly proportional to the torsional loss and thus to the pretension loss. Retightening the bolt to restore the original alignment will restore the pretension.

(c) **Future experimental studies:** Further experimental investigations will help establish the required intervals for friction-pad replacement or bolt replacement after several cycles of re-tensioning.

7 Conclusions

This paper proposes a new type of friction damper, the leaf spring rotational plate (LSRP) Damper, which combines the energy-dissipating characteristics of vehicle suspension leaf springs with rotational friction plates. The displacement demands generated by inter-story drift during ground motion can be effectively utilized to activate the damper's friction-based energy dissipation mechanisms.

A simplified mathematical formulation for the hysteretic strut force–displacement response of the LSRP damper was developed using equilibrium, compatibility, and energy-balance principles. The resulting theoretical response shows good agreement with the behavior obtained from numerical modeling.

The proposed damper can be designed and fabricated locally by considering realistic static friction coefficients, bolt pretension forces, and clamping forces, using the equations presented in this study. The equivalent viscous damping ratio of the LSRP damper is found to be proportional to the ratio between the strut force at the onset of leaf-plate slip and the maximum strut force corresponding to the peak displacement.

Energy dissipation is governed primarily by three contributing parameters: (1) frictional resistance at the core sliding plate, (2) the force required to initiate slip between the leaf plates by overcoming the clamping force, and (3) the deformation-related force in the individual leaf plates after inter-plate sliding occurs. The thickness of the leaf plates and core sliding plates can be selected to ensure that the system dissipates energy effectively without inducing plastic deformation in the plates.

Because a simplified friction model was used in the theoretical formulation, some discrepancies are observed when comparing its results with those obtained from the numerical model. Correction coefficients have been proposed to address these differences, but their accurate values should be established through further studies. This study considered three friction coefficients0.2, 0.3, and 0.5 and therefore recommends experimental evaluation of the realistic friction coefficients between the selected friction pad and steel plates.

Potential losses in bolt prestress after repeated cyclic loading also require experimental investigation. Such studies would allow the development of a reliable schedule for periodic bolt re-tensioning or for determining when the friction pad and bolts should be replaced.

Additionally, the leaf plates may be intentionally designed to undergo limited yielding to enhance the energy dissipation capacity of the damper. Further research is recommended to evaluate this design option.

Since the LSRP damper is displacement-sensitive, it can be installed in building structures between points of relative drift, similar to the locations typically used for diagonal bracing. The device can also be applied in bridges, with one anchor point connected to the abutment or pier and the other to the bottom flange of the bridge girder. In this configuration, the relative displacement between the superstructure and substructure serves as the input displacement, enabling the damper to effectively reduce the forces transmitted to the bridge substructure.

Acknowledgement: Not applicable.

Funding Statement: The authors received no specific funding for this study.

Author Contributions: The authors confirm contribution to the paper as follows: Conceptualization, methodology, writing original draft, writing review & editing: Radha Krishna Mallik; review of the paper and comments and suggestions for the improvement of research quality: Gokarna Bahadur Motra; review of the paper and comments and suggestions for the improvement of research quality: Krishna Shrestha. All authors reviewed the results and approved the final version of the manuscript.

Availability of Data and Materials: Not applicable.

Ethics Approval: Not applicable.

Conflicts of Interest: The authors declare no conflicts of interest to report regarding the present study.

References

1. Popov EP, Yang TS, Grigorian CE. New directions in structural seismic designs. Earthq Spectra. 1993;9(4):845–75. doi:10.1193/1.1585743.
2. Pall AS, Marsh C. Response of friction damped braced frames. J Struct Div. 1982;108(6):1313–23. doi:10.1061/jsdeag.0005968.
3. Symans MD, Charney FA, Whittaker AS, Constantinou MC, Kircher CA, Johnson MW, et al. Energy dissipation systems for seismic applications: current practice and recent developments. J Struct Eng. 2008;134(1):3–21. doi:10.1061/(asce)0733-9445(2008)134:1(3).
4. Habibi A, Chan RWK, Albermani F. Energy-based design method for seismic retrofitting with passive energy dissipation systems. Eng Struct. 2013;46:77–86. doi:10.1016/j.engstruct.2012.07.011.
5. Saaed TE, Nikolakopoulos G, Jonasson JE, Hedlund H. A state-of-the-art review of structural control systems. J Vib Control. 2015;21(5):919–37. doi:10.1177/1077546313478294.
6. Chen WF, Lui EM. Handbook of structural engineering. Boca Raton, FL, USA: CRC Press; 2005. 1768 p.
7. Constantinou MC, Symans MD. Seismic response of structures with supplemental damping. Struct Des Tall Build. 1993;2(2):77–92. doi:10.1002/tal.4320020202.
8. Merritt S, Uang CM, Benzoni G. Subassemblage testing of star seismic buckling-restrained braces. San Diego, CA, USA: University of California; 2003.
9. Black CJ, Makris N, Aiken ID. Component testing, seismic evaluation and characterization of buckling-restrained braces. J Struct Eng. 2004;130(6):880–94. doi:10.1061/(asce)0733-9445(2004)130:6(880).
10. Fahnestock LA, Ricles JM, Sause R. Experimental evaluation of a large-scale buckling-restrained braced frame. J Struct Eng. 2007;133(9):1205–14. doi:10.1061/(asce)0733-9445(2007)133:9(1205).
11. Kiggins S, Uang CM. Reducing residual drift of buckling-restrained braced frames as a dual system. Eng Struct. 2006;28(11):1525–32. doi:10.1016/j.engstruct.2005.10.023.
12. Erochko J, Christopoulos C, Tremblay R, Choi H. Residual drift response of SMRFs and BRB frames in steel buildings designed according to ASCE 7-05. J Struct Eng. 2011;137(5):589–99. doi:10.1061/(asce)st.1943-541x.0000296.
13. Constantinou MC, Symans M. Experimental and analytical investigation of seismic response of structures with supplemental fluid viscous dampers [dissertation]. New York, NY, USA: University at Buffalo; 1992.
14. Makris N, Roussos Y, Whittaker A, Kelly J. Viscous heating of fluid dampers during seismic and wind excitations: analytical solutions and design formulae. Berkeley, CA, USA: University of California; 1997.
15. Pall AS. Limited slip bolted joints: a device to control the seismic response of large panel structures [dissertation]. Montreal, QC, Canada: Concordia University; 1979.
16. Filiatrault A, Tremblay R, Kar R. Performance evaluation of friction spring seismic damper. J Struct Eng. 2000;126(4):491–9. doi:10.1061/(asce)0733-9445(2000)126:4(491).
17. Filiatrault A, Cherry S. Performance evaluation of friction damped braced steel frames under simulated earthquake loads. Earthq Spectra. 1987;3(1):57–78. doi:10.1193/1.1585419.
18. Aiken ID, Kelly J, Pall A. Seismic response of a nine-story steel frame with friction damped cross-bracing [Internet]. Available from: https://www.palldynamics.com/pdf/32Pall2.pdf.
19. Aiken I, Kelly J. Earthquake simulator testing and analytical studies of two energy-absorbing systems for multi-story structures [dissertation]. Berkeley, CA, USA: University of California; 1990.
20. Yang TS, Popov EP. Experimental and analytical studies of steel connections and energy dissipators. Berkeley, CA, USA: University of California; 1995.
21. Tirca L, Serban O, Tremblay R, Jiang Y, Chen L. Seismic design, analysis and testing of a friction steel braced frame system for multi-storey buildings in Vancouver. Key Eng Mater. 2018;763:1077–86. doi:10.4028/www.scientific.net/kem.763.1077.
22. Mualla IH, Belev B. Performance of steel frames with a new friction damper device under earthquake excitation. Eng Struct. 2002;24(3):365–71. doi:10.1016/S0141-0296(01)00102-X.
23. Liao WI, Mualla I, Loh CH. Shaking-table test of a friction-damped frame structure. Struct Des Tall Spec Build. 2004;13(1):45–54. doi:10.1002/tal.232.

24. Leung H, Clifton G, Khoo HH, Macrae G. Experimental studies of eccentrically braced frame with rotational active links. In: Proceedings of the 8th International Conference on Behavior of Steel Structures in Seismic Areas; 2015 Jul 1–3; Shanghai, China.
25. Clifton GC. Semi-rigid joints for moment-resisting steel framed seismic-resisting systems [dissertation]. Auckland, New Zealand: University of Auckland; 2005.
26. MacRae GA, Clifton GC, Mackinven H, Mago N, Butterworth J, Pampanin S. The sliding hinge joint moment connection. Bull N Z Soc Earthq Eng. 2010;43(3):202–12. doi:10.5459/bnzsee.43.3.202-212.
27. Latour M, Piluso V, Rizzano G. Free from damage beam-to-column joints: testing and design of DST connections with friction pads. Eng Struct. 2015;85:219–33. doi:10.1016/j.engstruct.2014.12.019.
28. Morgen BG, Kurama YC. A friction damper for post-tensioned precast concrete moment frames. PCI J. 2004;49(4):112–33. doi:10.15554/pcij.07012004.112.133.
29. Kim HJ, Christopoulos C. Friction damped posttensioned self-centering steel moment-resisting frames. J Struct Eng. 2008;134(11):1768–79. doi:10.1061/(asce)0733-9445(2008)134:11(1768).
30. Wolski M, Ricles JM, Sause R. Seismic resistant self-centering steel moment resisting frame with bottom flange friction devices. In: Proceedings of the 5th International Conference on Behavior of Steel Structures in Seismic Areas; 2006 Aug 14–17; Yokohama, Japan. p. 481–7.
31. Borzouie J, MacRae GA, Chase JG, Rodgers GW, Clifton GC. Experimental studies on cyclic performance of column base strong axis-aligned asymmetric friction connections. J Struct Eng. 2016;142:04015078. doi:10.1061/(asce)st.1943-541x.0001327.
32. Freddi F, Dimopoulos CA, Karavasilis TL. Rocking damage-free steel column base with friction devices: design procedure and numerical evaluation. Earthq Eng Struct Dyn. 2017;46(14):2281–300. doi:10.1002/eqe.2904.
33. Golondrino JC, MacRae G, Clifton C. Behaviour of asymmetrical friction connections using different shim materials [Internet]. Available from: https://www.nzsee.org.nz/db/2012/Paper100.pdf.
34. Golondrino JC, MacRae G, Chase J, Rodgers G, Clifton C. Clamping force effects on the behaviour of asymmetrical friction connections (afc). In: Proceedings of the 15th World Conference on Earthquake Engineering (15WCEE); 2012 Sep 24–28; Lisbon, Portugal.
35. Khoo HH, Clifton C, Butterworth J, MacRae G, Ferguson G. Influence of steel shim hardness on the Sliding Hinge Joint performance. J Constr Steel Res. 2012;72:119–29. doi:10.1016/j.jcsr.2011.11.009.
36. Latour M, Piluso V, Rizzano G. Experimental analysis on friction materials for supplemental damping devices. Constr Build Mater. 2014;65:159–76. doi:10.1016/j.conbuildmat.2014.04.092.
37. Rojas P, Ricles JM, Sause R. Seismic performance of post-tensioned steel moment resisting frames with friction devices. J Struct Eng. 2005;131(4):529–40. doi:10.1061/(asce)0733-9445(2005)131:.
38. Wolski M, Ricles JM, Sause R. Experimental study of a self-centering beam–column connection with bottom flange friction device. J Struct Eng. 2009;135(5):479–88. doi:10.1061/(asce)st.1943-541x.0000006.
39. Ono S, Nakahira K, Tsujioka S, Uno N. Energy absorption capacity of thermally sprayed aluminum friction dampers. J Therm Spray Technol. 1996;5(3):303–9. doi:10.1007/BF02645882.
40. Wolff ED. Frictional heating in sliding bearings and an experimental study of high friction materials [dissertation]. New York, NY, USA: University at Buffalo; 1999.
41. Paronesso M, Lignos DG. Experimental study of sliding friction damper with composite materials for earthquake resistant structures. Eng Struct. 2021;248:113063. doi:10.1016/j.engstruct.2021.113063.
42. Jiang F, Xu G, Liu J, Dang S, Irshad Z, Yue Y, et al. Investigation on influence of friction plate material properties on hysteretic performance and stability of friction dampers. Buildings. 2025;15(18):3418. doi:10.3390/buildings15183418.
43. Gao J, Wang CL, Meng S, Zeng B. Performance evaluation of friction dampers considering different metal pairs and loading rates. J Constr Steel Res. 2023;204:107859. doi:10.1016/j.jcsr.2023.107859.
44. Yan L, Zhang C. Hysteretic performance of square rotational friction damper. Adv Struct Eng. 2025;28(10):1843–57. doi:10.1177/13694332251319095.

45. Shalchi Toosi M, Hojatkashani A, Haji Najafi L, Adib Ramezani M. Revealing seismic performance: exploring an innovative brace–brake pad friction damper through experimental and numerical approaches. J Struct Des Constr. 2025;30(3):04025050. doi:10.1061/jsdccc.sceng-1712.
46. Xu W, Cai Y, Liu Y, Zhang T, Lu Y. Experimental and numerical study of a metal-friction hybrid damper. Structures. 2024;62:106256. doi:10.1016/j.istruc.2024.106256.
47. Yang W, Cao S, Liu W, Dang X. Mechanical properties of a novel friction dampers incorporated with buckling restrained shape memory alloy bars. Adv Bridge Eng. 2024;5(1):21. doi:10.1186/s43251-024-00133-5.
48. Pall A, Pall RT. Performance based design using pall friction dampers-an economical design solution. In: Proceedings of the 13th World Conference on Earthquake Engineering; 2004 Aug 1–6; Vancouver, BC, Canada. 1955 p.
49. Etedali S, Akbari M, Seifi M. MOCS-based optimum design of TMD and FTMD for tall buildings under near-field earthquakes including SSI effects. Soil Dyn Earthq Eng. 2019;119:36–50. doi:10.1016/j.soildyn.2018.12.027.
50. Nouri Y, Ghasemi Jouneghani H, Shirkhani A, Hemati E, Hemati SA, Hajirasouliha I. Seismic retrofit of steel moment frames with arc and ring yielding dampers: a probabilistic loss assessment using FEMA P-58. Structures. 2025;76:108898. doi:10.1016/j.istruc.2025.108898.
51. Xu G, Guo T, Li A, Wang S, Zhang R, Zhu R, et al. Review on self-centering damper for seismic resilient building structures. Structures. 2023;54:58–77. doi:10.1016/j.istruc.2023.05.046.
52. Javidan MM, Ahmad RN, Chun S, Kim J. Seismic retrofit of framed structures using a steel frame with springs and friction dampers. Structures. 2024;64:106555. doi:10.1016/j.istruc.2024.106555.
53. Montazeri M, Namiranian P, Pasand AA, Aceto L. Seismic performance of isolated buildings with friction spring damper. Structures. 2023;55:1481–96. doi:10.1016/j.istruc.2023.06.116.
54. Yang C, Xie L, Li A, Liu B, He Y. Experimental study of rotational friction damper for seismic response control: friction material comparison and configuration optimization. Case Stud Constr Mater. 2024;21:e03825. doi:10.1016/j.cscm.2024.e03825.
55. Yang C, Xie L, Liu Q, Li A, Wang X, Liu Q. Experimental and numerical investigations of a novel parallel double-stage crawler-track-shaped shear damper. Thin Walled Struct. 2024;195:111428. doi:10.1016/j.tws.2023.111428.
56. Grossi E, Zerbin M, Aprile A, de Risi R, de Luca F. Conceptual study of an innovative friction damper for the seismic retrofit of precast RC structures with poor connections. Structures. 2024;67:106960. doi:10.1016/j.istruc.2024.106960.
57. Addala MB, Bhalla S, Madan A. Performance based design of a new hybrid passive energy dissipation device for vibration control of reinforced concrete frames subjected to broad-ranging earthquake ground excitations. Adv Struct Eng. 2022;25(4):895–912. doi:10.1177/13694332211052350.
58. Mustafa ZNE, Majima R, Saito T. Evaluation of viscoelastic and rotational friction dampers for coupled shear wall system. Appl Sci. 2025;15(15):8185. doi:10.3390/app15158185.
59. Guo J, Li H, Zhang C, Chu S, Dang X. Effect of an innovative friction damper on seismic responses of a continuous girder bridge under near-fault excitations. Buildings. 2022;12(7):1019. doi:10.3390/buildings12071019.
60. Liang L, Feng Z, Xu Y, Chen Z, Liang L. A parallel scheme of friction dampers and viscous dampers for girder-end longitudinal displacement control of a long-span suspension bridge under operational and seismic conditions. Buildings. 2023;13(2):412. doi:10.3390/buildings13020412.
61. Yue Y, Zhang Y, Li W, Li C, Zhang Y, Jiang F, et al. Experimental and numerical study of friction damper parallel composite buckling-restrained bracing. Structures. 2025;78:109166. doi:10.1016/j.istruc.2025.109166.
62. Wu Q, Jia C, Liu WG, Sun J, Chen X, Zhu H, et al. Experimental and numerical study on a novel viscoelastic-friction composite damper. Structures. 2025;75:108840. doi:10.1016/j.istruc.2025.108840.
63. Jacobsen LS. Steady forced vibrations as influenced by damping, transactions. Vol. 52. New York, NY, USA: ASCE; 1968. p. 103–14.